

Politecnico di Bari

Repository Istituzionale dei Prodotti della Ricerca del Politecnico di Bari

Triphenylphosphane Pt(II) complexes containing biologically active natural polyphenols: Synthesis, crystal structure, molecular modeling and cytotoxic studies

This is a pre-print of the following article

Original Citation:
Triphenylphosphane Pt(II) complexes containing biologically active natural polyphenols: Synthesis, crystal structure, molecular modeling and cytotoxic studies / Dell'Anna, M.M., Censi, V., Carrozzini, B., Caliandro, R., Denora, N., Franco, M., Veclani, D., Melchior, A., Tolazzi, M., Mastrorilli, P.. - In: JOURNAL OF INORGANIC BIOCHEMISTRY. - ISSN 0162-0134. - STAMPA. - 163:(2016), pp. 346-361. [10.1016/j.jinorgbio.2016.08.006]

Availability:
This version is available at http://hdl.handle.net/11589/79999 since: 2021-03-11

Published version
DOI:10.1016/j.jinorgbio.2016.08.006

Publisher:

Terms of use:

(Article begins on next page)

26 November 2026

Elsevier Editorial System(tm) for Journal of Inorganic Biochemistry

Manuscript Draft

Manuscript Number:

Title: Triphenylphosphane Pt(II) complexes containing biologically active natural polyphenols: synthesis, crystal structure, molecular modeling and cytotoxic studies

Article Type: SI: ISMEC 2015

Keywords: Platinum(II) complexes; Cytotoxic activity; Natural Polyphenols; Flavonoids; DFT.

Corresponding Author: Dr. Maria Michela Michela Dell'Anna, Ph.D.

Corresponding Author's Institution: Politecnico di Bari

First Author: Maria Michela Michela Dell'Anna, Ph.D.

Order of Authors: Maria Michela Michela Dell'Anna, Ph.D.; Valentina Censi, PhD student; Benedetta Carrozzini, Dr.; Rocco Caliandro, Dr.; Nunzio Denora, Dr.; Massimo Franco, Prof.; Daniele Veclani, PhD student; Andrea Melchior, Prof.; Marilena Tolazzi, Prof.; Piero Mastrorilli, Prof.

Abstract: Platinum complexes bearing phosphane ligands in cis configuration with deprotonated flavonoids (3-hydroxyflavone, quercetin) and deprotonated ethyl gallate were synthesized starting from cis-[PtCl2(PPh3)2]. In all cases, O,O' chelate structures were obtained. While quercetin and ethyl gallate complexes are quite stable in solution, the 3-hydroxyflavonate complex undergoes a slow aerobic photodegradation in solution with formation of salicylic and benzoic acids. The XRD structures of quercetin and ethyl gallate complexes are reported. Cell cycle studies (in the dark) of the complexes in two human cell lines revealed that the cytotoxic activity of the complex bearing 3-hydroxyflavonate is higher than those exhibited by 3-hydroxyflavone or by cis-[PtCl2(PPh3)2] alone, thus showing a synergic effect between the ligand and the starting platinum complex. DFT studies on the hydrolysis pathway for the 3-hydroxyflavone and ethyl gallate complexes explained the different cytotoxic activity observed for the two compounds on the basis of the different intermediates formed during hydrolysis (relatively inert hydroxy Pt complexes for ethyl gallate and monoaqua complexes for 3-hydroxyflavone).

Dear Editor,

on behalf of all authors we have proceeded with the online submission of the paper entitled:

"**Triphenylphosphane Pt(II) complexes containing biologically active natural polyphenols: synthesis, crystal structure, molecular modeling and cytotoxic studies"** by Maria Michela Dell'Anna, Valentina Censi, Benedetta Carrozzini, Rocco Caliandro, Nunzio Denora, Massimo Franco, Daniele Veclani, Andrea Melchior, Marilena Tolazzi, and Piero Mastrorilli.

We would like that this paper would be included in the *Journal of Inorganic Biochemistry* Special Issue dedicated to the ISMEC2015 conference (June 24-28 Wroclaw, Poland) where Andrea Melchior attended as invited lecturer.

This manuscript reports on the synthesis and characterization of platinum complexes bearing phosphane ligands in *cis* configuration with deprotonated flavonoids (3-hydroxyflavone, quercetin) and deprotonated ethyl gallate. Cell cycle studies of the complexes in two human cell lines revealed that the cytotoxic activity of the complex bearing 3-hydroxyflavone is higher than those exhibited by 3-hydroxyflavone or by *cis*-$[PtCl_2(PPh_3)_2]$ alone, thus showing a synergic effect between the ligand and the starting platinum complex. A similar synergic cytotoxic effect was not observed for the platinum complex bearing ethyl gallate. DFT studies on the hydrolysis pathway for the 3-hydroxyflavone and ethyl gallate complexes suggest a possible factor of the different cytotoxic activity of the two compounds on the basis of the different intermediates formed during hydrolysis (relatively inert hydroxy Pt complexes for ethyl gallate and monoaqua complexes for 3-hydroxyflavone).

We hope you can find this manuscript suitable for publication in *Journal of Inorganic Biochemistry* in the ISMEC2015 Special Issue.

Best Regards,

Maria Michela Dell'Anna



Andrea Melchior

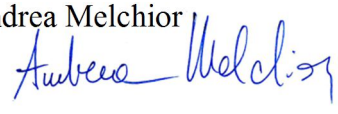

Pictogram for the Graphical Abstract

Click here to download high resolution image

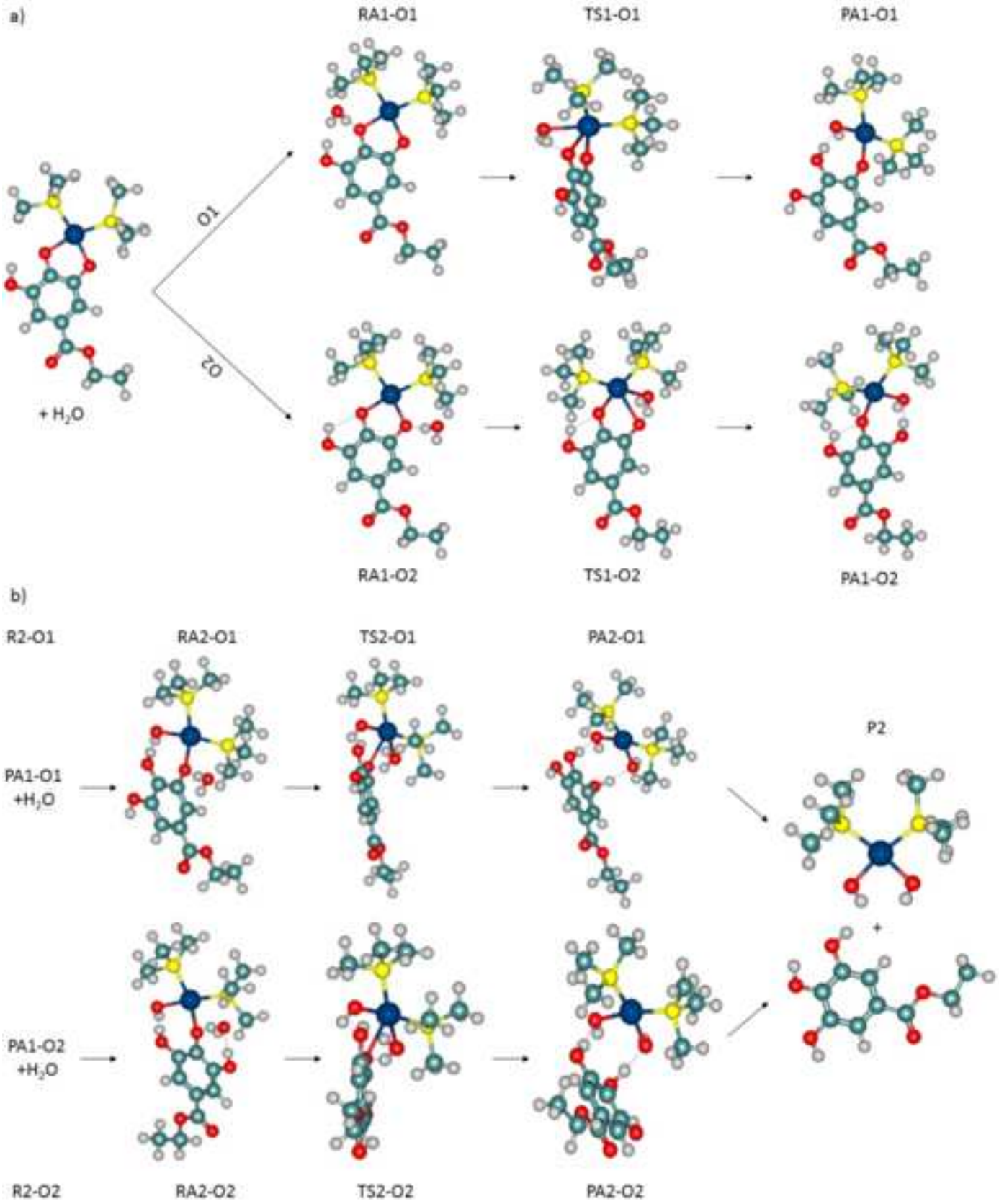

Graphical Abstract (synopsis)

Triphenylphosphane platinum complexes bearing the deprotonated form of 3-hydroxyflavone, quercetin and ethyl gallate were synthesized. DFT studies on the hydrolysis pathway for the 3-hydroxyflavone and ethyl gallate complexes explained the different cytotoxic activity observed for the two compounds on the basis of the different intermediates formed during hydrolysis.

Highlights

- Platinum complexes bearing natural biologically active polyphenols were synthesized
- XRD structures and cytotoxicity studies are reported
- A cytotoxic synergic effect was observed for the Pt 3-hydroxyflavonate complex
- DFT studies indicate that the new complexes release their polyphenol in solution
- DFT studies on the hydrolysis pathway explain observed cytotoxic activities

*Manuscript
Click here to download Manuscript: manuscript.docx Click here to view linked References

Triphenylphosphane Pt(II) complexes containing biologically active natural polyphenols: synthesis, crystal structure, molecular modeling and cytotoxic studies.

Maria Michela Dell'Anna,*[a] Valentina Censi,[a] Benedetta Carrozzini,[b] Rocco Caliandro,[b] Nunzio Denora,[c] Massimo Franco,[c] Daniele Veclani,[d] Andrea Melchior,[d] Marilena Tolazzi,[d] and Piero Mastrorilli[a]

[a] DICATECh, Politecnico di Bari, via Orabona, 4 I-70125, Bari, Italy
e-mail: mariamichela.dellanna@poliba.it
[b] Institute of Crystallography CNR, via Amendola, 122/o I-70126, Bari, Italy
[c] Department of Pharmacy, University of Bari, via Orabona, 4 I-70125, Bari, Italy
[d] DPIA, University of Udine, via del Cotonificio 108, I-33100 Udine, Italy

Abstract

Platinum complexes bearing phosphane ligands in *cis* configuration with deprotonated flavonoids (3-hydroxyflavone, quercetin) and deprotonated ethyl gallate were synthesized starting from *cis*-$[PtCl_2(PPh_3)_2]$. In all cases, *O,O'* chelate structures were obtained. While quercetin and ethyl gallate complexes are quite stable in solution, the 3-hydroxyflavonate complex undergoes a slow aerobic photodegradation in solution with formation of salicylic and benzoic acids. The XRD structures of quercetin and ethyl gallate complexes are reported. Cell cycle studies (in the dark) of the complexes in two human cell lines revealed that the cytotoxic activity of the complex bearing 3-hydroxyflavonate is higher than those exhibited by 3-hydroxyflavone or by *cis*-$[PtCl_2(PPh_3)_2]$ alone, thus showing a synergic effect between the ligand and the starting platinum complex. DFT studies on the hydrolysis pathway for the 3-hydroxyflavone and ethyl gallate complexes explained the different cytotoxic activity observed for the two compounds on the basis of the different

intermediates formed during hydrolysis (relatively inert hydroxy Pt complexes for ethyl gallate and monoaqua complexes for 3-hydroxyflavone).

Keywords Platinum(II) complexes; Cytotoxic activity; Natural Polyphenols; Flavonoids; DFT.

1. Introduction

The discovery of antiproliferative activity of cisplatin by Rosenberg et al. [1] in 1965 contributed to the development of cancer chemotherapy. Today cisplatin is a widely used drug in chemotherapy, but its applicability has many disadvantages, as it causes many severe side effects including: nephrotoxicity, neurotoxicity, myelotoxicity, hematological toxicity and gastrointestinal reactions [2]. In addition, some tumors have acquired resistance to cisplatin, while others develop resistance after the initial treatment. In view of these limitations, research has been extended to other platinum complexes. A large number of platinum analogues have been tested during the last 30 years [3]. Unfortunately, the vast majority of these compounds were rejected in preclinical or early clinical stages of testing (only carboplatin and oxaliplatin, Scheme 1, are in world-wide clinical use) and the discovery of a new platinum drug more selective and less toxic than cisplatin is still highly desirable.

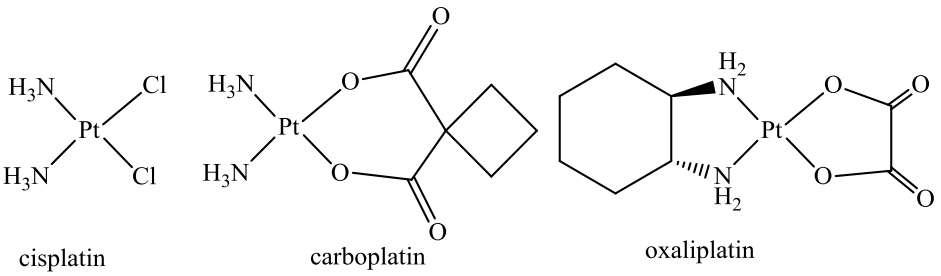

Scheme 1. Platinum based anticancer drugs used in clinical therapies.

Recently, the antitumor activity of dietary flavonoids (flavus = yellow), which are primarily benzo-γ-pyrone (phenylchromone) derivatives (Scheme 2), comprising a massive group of polyphenolic compounds [4] universally distributed in the plant kingdom, has been reviewed [5]. The pharmacological effects of flavonoids include induction of apoptosis, suppression of protein tyrosine kinase activity, antiproliferation, antimetastatic and antiinvasive effects, and anti-angiogenesis [5].

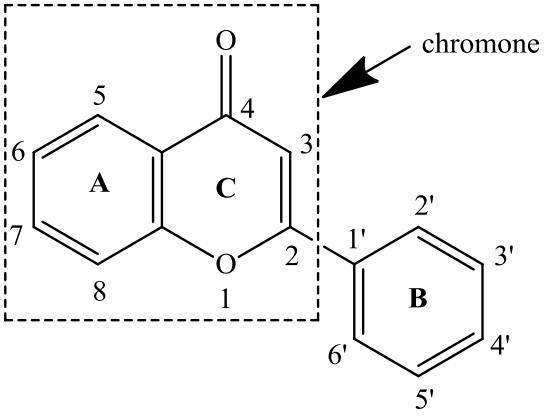

Scheme 2. Flavone backbone.

Because of structural differences, flavonoids are divided into eight different groups, being flavonols one of them. 3-Hydroxyflavone (Scheme 3a) is the backbone of all flavonols [6], while quercetin (Scheme 3b) is another very important flavonol with well-known anticancer activity [7]. Due to their polyphenolic structure, flavonols are effective metal ion chelators, playing a key role in the initiation of free radical and antioxidant processes [8]. Moreover flavonols can intercalate into deoxyribonucleic acid (DNA) as well as covalently bind to DNA and proteins [9]. As a result of these characteristics, flavonols have complex biological interactions and in some therapies they are combined with cisplatin increasing efficacy over individual treatments [10] and reducing side effects associated with cisplatin [11]. However, combinations of flavonols with platinum are poorly understood, although multiple theories currently exist trying to explain the interactions between cisplatin and flavonols [12].

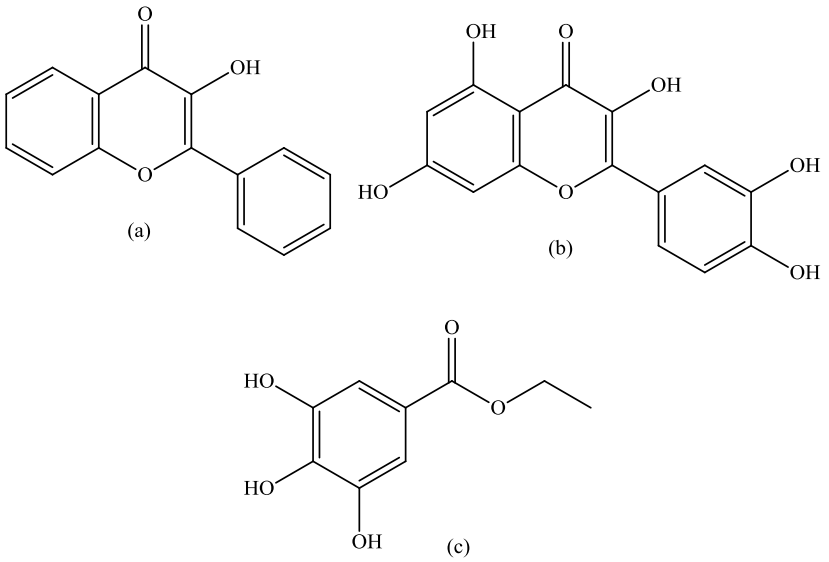

Scheme 3. (a) 3-Hydroxyflavone; (b) quercetin; (c) ethyl gallate.

Like flavonols, also plant phenols, such as ethyl gallate (Scheme 3c), have antitumor activity [13] and can effectively bind metal ions.

All these considerations prompted us to check whether platinum complexes of natural polyphenols would exhibit synergic cytotoxic activity. Although since the early 1980s scientists have investigated more than 40 metal–flavonoid complexes [14], to the best of our knowledge Pt(II) complexes with 3-hydroxyflavone and ethyl gallate as ligands have never been synthesized. On the contrary, the synthesis of a platinum(II) complex with quercetin has already been reported [15]. Its formula is *cis*-[$Pt(NH_3)_2$(que)] (que = dianion of quercetin) and a complexation of platinum(II) to the ligand through oxygen atoms at $C^{3'}$ and $C^{4'}$ was hypothesized, although no XRD neither citotoxicity studies were carried out.

Phosphane ligands with hydrophobic character have been shown to increase in some cases the cytotoxicity of their platinum complexes, possibly by enhancing the cellular membrane transfer process [16]. Interesting results were also obtained with platinum complexes bearing an amine and a phosphane ligand in *trans* position [17]. Although the total replacement of the usually employed amine carrier ligands (Scheme 1) for air and water stable triarylphosphanes may exhibit some

disadvantages (the major of them being that a tertiary phosphane cannot establish any hydrogen bond with the DNA backbone), however it has been found that triarylphosphane ligands may stabilize DNA-Pt adducts through π–π interactions occurring between the phosphane phenyl groups and the nucleobases [18]. Indeed, some examples exist on the interaction between DNA and bisphosphane platinum complexes [19]. In addition, PR_3 ligand has a kinetic *trans* effect stronger than NH_3, which can facilitate the leaving group displacement by H_2O in the human cell. The ligand release by hydrolysis is a key-step for the DNA-adduct formation and attracted numerous experimental studies[20]. Furthermore, in the last decade a variety of theoretical approaches have been applied to obtain an accurate picture of the hydrolysis mechanism of Pt(II)-based anticancer drugs and ultimately of the structure-activity relationship [21].In this framework, we started a project aiming at preparing new platinum complexes containing triphenylphosphane as carrier ligand and flavonolates or natural polyphenolates as leaving groups. Herein, we report on the synthesis, characterization, cytotoxicity and DFT studies of *cis*-[$Pt(PPh_3)_2$(que)] (**1**, que = dianion of quercetin), *cis*-[$Pt(PPh_3)_2$(3-Hfl)]Cl (**2**, 3-Hfl = monoanion of 3-hydroxyflavone), and *cis*-[$Pt(PPh_3)_2$(etga)] (**3**, etga = dianion of ethyl gallate).

2. Experimental Section

2.1. Material and methods.

Tap water was de-ionized by ionic exchange resins (Millipore) before use. All chemicals and solvents were purchased from commercial suppliers and used without further purification. *cis*-$Pt(PPh_3)_2Cl_2$ was synthetized according to literature procedures [22].

Melting points were determined with a Büchi Melting Point B-540 apparatus and are uncorrected. Elemental analyses were carried out with a Perkin Elmer 2400 CHN Elemental Analyser at the Microanalytical Laboratory of the University of Bari, Department of Pharmacy. IR spectra were recorded on a Bruker-Vector 22 spectrometer. NMR spectra were recorded on a BRUKER Avance

400 spectrometer; frequencies are referenced to Me_4Si (^1H and ^{13}C), 85% H_3PO_4 (^{31}P) and H_2PtCl_6 (^{195}Pt). The signal attributions and coupling constant assessment were made on the basis of a multinuclear NMR analysis of each compound including, besides 1D spectra, ^1H-^{31}P HMQC, ^1H-^{195}Pt HMQC, ^1H-^{13}C HSQC, ^1H-^{13}C HMBC and ^1H COSY. High resolution mass spectrometry (HR-MS) analyses were performed using a time-of-flight mass spectrometer equipped with an electrospray ion source (Bruker micrOTOF). The sample solutions were introduced by continuous infusion with the aid of a syringe pump at a flow rate of 180 μL/min. The instrument was operated at end plate offset −500 V and capillary −4500 V. Nebulizer pressure was 1.5 bar (N_2), and the drying gas (N_2) flow was 10 L/min. Capillary exit and skimmer 1 were 120 and 40 V, respectively. The drying gas temperature was set at 220°C. The software used for the simulations is Bruker Daltonics Data Analysis (version 3.3).

*2.2.Synthesis of cis-[Pt(PPh_3)$_2$(que)] (que = dianion of quercetin) (**1**)*

A solution of KOH (2.90 mmol, 162.7 mg) in ethanol (7.0 mL) kept at 40°C was added dropwise to a clear yellow solution of *cis*-[$PtCl_2(PPh_3)_2$] (1.45 mmol, 1.149 g) and quercetin (1.45 mmol, 0.439 g) in CH_2C1_2 (80 mL) at room temperature under stirring. After overnight stirring at room temperature, the resulting dark orange reaction mixture was filtered (in order to remove KCl) and dried under reduced pressure. The red orange residue was dissolved in CH_2Cl_2 (10 mL) and added of *n*-hexane (30 mL), which caused the formation of a red-orange precipitate. This solid was filtered after overnight cooling at 4°C, washed with *n*-hexane (3 x 10 mL) and dried under vacuum.

Yield: 1.073 g, 72 %. Mp=212.5°C (dec).

Relevant ^1H and $^{13}C\{^1H\}$ NMR features are reported in tables 3 and 2, respectively, except those belonging to PPh_3 groups. PPh_3 region: ^1H NMR (400 MHz, dmso-d_6, 25 °C) δ = 7.45 ppm (m, 12 H, H_{ortho}), 7.42 ppm (m, 6 H, H_{para}), 7.29 ppm (m, 12 H, H_{meta}); $^{13}C\{^1H\}$ NMR (100 MHz dmso-d_6, 25 °C) δ = 134.7 ppm (s, C_{ortho}), 131.6 (s, C_{para}), 128.8 (s, C_{ipso}), 128.6 (s, C_{meta}).

$^{31}P\{^{1}H\}$ NMR (121.5 MHz, dmso-d_6, 25 °C): δ = 9.6 ppm (d, $^{2}J_{PP}$ = 23 Hz, $^{1}J_{PtP}$ = 3565 Hz); 8.3 ppm (d, $^{2}J_{PP}$ = 23 Hz, $^{1}J_{PtP}$ = 3600 Hz).

$^{195}Pt\{^{1}H\}$ NMR (85.99 MHz, dmso-d_6, 25 °C): δ = –4062 ppm (dd, $^{1}J_{PtP}$ = 3565 Hz, $^{1}J_{PtP}$ = 3600 Hz).

IR (KBr, cm^{-1}): 3372-3633 (b, m, O-H), 3058 (m, C-H), 1650 (s, C=O), 1617 (s, C=C), 1515 (s, C=C), 1491 (s, C=C), 1426 (s, C=C), 1354 (m, O-H), 1270 (s, C-O-C), 1162 (m, O-H), 1099 (m, C-H), 997 (m, C-O-C), 741 (m, C-H), 530 (m, Pt-O).

HRMS (ESI, acetonitrile, positive ion mode) *m/z*: calcd. for $C_{51}H_{38}O_7P_2Pt$ $[M]^+$ 1019.1740; found 1019.1681. HRMS (ESI, acetonitrile, negative ion mode) *m/z*: calcd. for $C_{51}H_{37}O_7P_2Pt$ [M□H]□ 1018.1672; found 1018.1678.

*2.3.Synthesis of cis-[Pt(PPh$_3$)$_2$(3-Hfl)]Cl (3-Hfl = monoanion of 3-hydroxyflavone) (**2**)*

A solution of KOH (0.64 mmol, 35.9 mg) in ethanol (4.5 mL) kept at 40 °C was added dropwise to a clear yellow solution of *cis*-$[PtCl_2(PPh_3)_2]$ (0.64 mmol, 506.0 mg) and 3-hydroxyflavone (0.64 mmol, 152.5 mg) in CH_2Cl_2 (40 mL) at room temperature under stirring. After overnight stirring at room temperature, the reaction mixture was filtered to remove KCl and the resulting orange solution was concentrated to 2 mL under reduced pressure and added of ethanol (10 mL). Addition of pentane (30 mL) caused the precipitation of an orange solid from the solution. The solid was washed with *n*-pentane (3 x 10 mL) and dried under vacuum.

Yield: 0.403 g, 63.5 %. Anal. Calcd. for **2**, $C_{51}H_{39}O_3P_2PtCl$: C, 61.68; H, 3.93. Found: C, 61.09; H, 4.18. Mp=219.1°C (dec).

^{1}H and $^{13}C\{^{1}H\}$ NMR features are reported in tables 3 and 2, respectively, except those belonging to PPh_3 groups. PPh_3 region: ^{1}H NMR (400 MHz, dmso-d_6, 25 °C) δ = 7.78–7.16 ppm; $^{13}C\{^{1}H\}$ NMR (100 MHz, dmso-d_6, 25 °C) δ = 135–128 ppm.

$^{31}P\{^{1}H\}$ NMR (121.5 MHz, dmso-d_6, 25 °C): δ = 8.60 ppm (d, $^{2}J_{PP}$ = 24 Hz, $^{1}J_{PtP}$ = 3667 Hz); 4.26 ppm (d, $^{2}J_{PP}$ = 24 Hz, $^{1}J_{PtP}$ = 3991 Hz).

$^{195}Pt\{^{1}H\}$ NMR (85.99 MHz, dmso-d_6, 25 °C): δ = –4077 ppm (dd, $^{1}J_{PtP}$ = 3667 Hz, $^{1}J_{PtP}$ = 3991 Hz).

IR (nujol mull, cm^{1}): 3059 (m, C-H), 1613 (s, C=O), 1568 (s, C=C), 1257 (m, C-O-C), 1093 (m, C-H), 996 (m, C-O-C), 755 (s, C-H), 515 (m, Pt-O).

HRMS (ESI, acetonitrile, positive ion mode) *m/z*: calcd. for $C_{51}H_{39}O_3P_2Pt$ $[M\text{-}Cl]^+$ 956.2021; found 956.2021.

*2.4.Synthesis of cis-[Pt(PPh$_3$)$_2$(etga)] (etga = dianion of ethyl gallate) (**3**)*

A solution of KOH (1.29 mmol, 72.4 mg) in ethanol (4.5 mL) kept at 40 °C was added dropwise to a clear yellow solution of *cis*-$[PtCl_2(PPh_3)_2]$ (0.64 mmol, 0.505 g) and ethyl gallate (0.64 mmol, 126.8 mg) in CH_2Cl_2 (40 mL) at room temperature under stirring. After overnight stirring at room temperature, the reaction mixture was filtered to remove KCl and the resulting solution was evaporated under reduced pressure and added of CH_2Cl_2 (10 mL). Addition of *n*-pentane (30 mL) caused the precipitation of a yellow solid from the dark yellow solution. The solid was washed with *n*-pentane (3 x 10 mL) and dried under vacuum.

Yield: 0.376 g, 69.1%. Anal. Calcd. for **3**, $C_{39}H_{44}O_5P_2Pt$: C 58.97, H 4.15; found C 58.41, H 4.22.

IR (nujol mull, cm^{-1}): 3496 (s, O-H), 3049 (m, C-H), 2000-1813 (w, aromatic overtone), 1688 (s, C=O), 1591 (s, C=C), 596 (s, Pt-O).

^{1}H NMR (400 MHz dmso-d_6, 25 °C) δ = 7.44 ppm (m, 12 H, $H_{ortho,}$ PPh_3), 7.43 ppm (m, 6 H, $H_{para,}$ PPh_3), 7.28 ppm (m, 12 H, $H_{meta,}$ PPh_3), 6.56 ppm (s, 1H, 6-H), 6.41 ppm (s, 1H, 2-H), 5.60 ppm (s, 1H, 5-H), 4.10 ppm (q, 2H, CH_2, $^{3}J_{HH}$ = 7.1 Hz), 1.20 ppm (t, 3H, CH_3, $^{3}J_{HH}$ = 7.1 Hz). $^{13}C\{^{1}H\}$ NMR (100 MHz dmso-d_6, 25 °C) δ = 167.2 ppm (s, CO), 163.1 ppm (s, C^3), 154.6 ppm (s, C^4), 144.6 (s, C^5), 134.8 ppm (s, $C_{ortho,}$ PPh_3), 131.8 ppm (s, $C_{para,}$ PPh_3), 128.8 ppm (s, $C_{meta,}$ PPh_3),

128.5 ppm (s, $C_{ipso,}$ PPh_3), 116.8 ppm (s, C^1), 109.6 ppm (s, C^2), 104.3 ppm (s, C^6), 59.9 8s, CH_2), 14.8 (s, CH_3).

$^{31}P\{^1H\}$ NMR (121.5 MHz, dmso-d_6, 25 °C): δ = 11.2 ppm (d,$^1J_{PtP}$ = 3552 Hz, $^2J_{PP}$ = 24 Hz); 6.4 ppm (d,$^1J_{PtP}$ = 3660 Hz, $^2J_{PP}$ = 24 Hz).

^{195}Pt NMR (85.99 MHz, dmso-d_6, 25 °C): δ = –4062 ppm (*pseudo t*).

HRMS (ESI, acetonitrile, positive ion mode) *m/z*: calcd. for $C_{45}H_{38}O_5P_2Pt$ $[M]^+$ 916.1841; found 916.1845; calcd. for $C_{45}H_{38}O_5P_2PtNa$ $[M+Na]^+$ 938.1739; found 938.1755; calcd. for $C_{45}H_{38}O_5P_2PtK$ $[M+K]^+$ 954.1478; found 954.1496.

*2.5.Photodegradation of **2***

Four NMR tubes were filled with a dmso-d_6 solution (0.6 mL) of **2** (10^{-6} mol), two of them under aerobic conditions and the others under nitrogen atmosphere, using de-aerated solvent. Each tube was then capped and a ^1H NMR spectrum was immediately recorded. Afterwards, one of the NMR tubes under air and one under nitrogen were placed in the dark, leaving the others in the daylight. The solutions were checked by ^1H NMR after five days.

2.6.Crystallographic analysis

Compounds **1** and **3** underwent batch crystallization, by slow diffusion of *n*-pentane in a solution of tetrahydrofuran containing the respective complex. Crystals suitable for diffraction analysis were obtained after 2 weeks.

The single-crystal X-ray diffraction data for crystals **1** and **3** were collected on a Kappa CCD Nonius area detector diffractometer, in φ and ω scans mode. Reflection data were measured at 293 K, using graphite monochromated Mo Kα radiation (λ = 0.71073 Å). Data were corrected for Lorentz and polarisation effects [23] and for absorption [24].

The structures were solved by the Patterson deconvolution procedure of SIR2014 [25] and refined by the full-matrix least-squares technique based on F^2 with SHELXL2014/7 [26], using collected reflections with $I \geq 2\sigma(I)$; up to 0.85Å (crystal **1**) and 0.83Å (crystal **3**) resolution; measured reflections with $|(I_{obs} - I_{cal})/\mathrm{SigW}(I)| > 10$ were excluded during the refinement process. The non-hydrogen atoms were refined with anisotropic thermal parameters. The aromatic, methyl and hydroxyl hydrogen atoms were placed in calculated positions, refined with isotropic thermal parameters [$U(H) = 1.2U\mathrm{eq(C)}$, $U(H) = 1.5U\mathrm{eq(Me,O)}$], and allowed to ride on their carrier atoms. The SQUEEZE routine in PLATON [27],designed to treat electron density of disordered and diffused solvents, was applied to improve the structure refinement for **1**. Crystallographic data collection and refinement parameters are given in Table 1. Molecular graphics were generated by using MERCURY CSD 2.0 [28] and JAV [29]. Two atoms separated by less than the sum of their Van der Waals radii have been considered in contact: for intermolecular contacts the two atoms must belong to different symmetry-equivalent molecules, for intramolecular contacts the additional requirement is that the two atoms must be separated by more than 4 bonds. The cif files CCDC-1430059 for **1** and -1430058 for **3** contain the supplementary crystallographic data for this paper. These data can be obtained free of charge from the Cambridge Crystallographic Data Centre.

Table 1. Crystal data, experimental details and refinement parameters for **1** and **3**.

	1	**3**
Chemical formula	$C_{51}H_{38}O_7P_2Pt$	$C_{45}H_{38}O_5P_2Pt$
M_r	1019.84	915.78
Crystal system	Orthorhombic	Triclinic
Space group	*Pbnb*	$P\bar{1}$
a, *b*, *c* (Å)	15.372, 22.066, 32.445	11.038, 12.269, 15.242
α, β, γ (°)	90.00, 90.00, 90.00	72.53, 85.17, 89.25
V (Å^3)	11005.3	1961.9
Z	8	2
F(000)	4064	912
D_x (Mg m^{-3})	1.231	1.550
μ (mm^{-1})	2.65	3.70
Crystal shape	Prismatic	Rod-shaped
Colour	Red	Pale yellow
Crystal size (mm)	0.25 × 0.25 × 0.10	0.25 × 0.13 × 0.03
No. of measured reflections	87739	20140
No. of independent reflections	9323	7162
R_{int}	0.175	0.127
θ values (°)	θ_{max} = 24.7, θ_{min} = 2.0	θ_{max} = 25.4, θ_{min} = 2.6

$R[F^2 > 2\sigma(F^2)]$, $wR(F^2)$, S	0.064, 0.178, 0.98	0.060, 0.167, 0.89
No. of observed reflections [$I > 2\sigma(I)$]	5316	4984
No. of parameters	553	479
$\Delta\rho_{max}$, $\Delta\rho_{min}$ (e Å^{-3})	2.01, −0.73	0.90, −1.54

2.7. Computational details

In this work we studied the hydrolysis reaction for *cis*-[Pt(PMe$_3$)$_2$(etga)], *cis*-[Pt(PMe$_3$)$_2$(3-Hfl)]$^+$, and *cis*-[PtCl$_2$(PMe$_3$)$_2$] by means of Density Functional Theory (DFT) calculations using mPW1PW91 functional, which has been previously demonstrated to provide reliable structures and energies for cisplatin and its derivatives [**Error! Bookmark not defined.**a]. Geometry optimizations were carried out in vacuum and with a 6-31+G(d) basis set for all atoms except the platinum atom, which was described by the quasi-relativistic Stuttgart–Dresden pseudopotential (SDD) [30]. In order to confirm that stationary points were actually minima or transition state geometries, the analytical calculation of second derivatives of the energy and vibrational frequency analysis were carried out. Potential energy profiles were estimated from total electronic energies and adding zero point energy (ZPE) and thermal corrections at 298.15 K.

DFT calculations were performed with the Gaussian 09 program [31]. Phenyls in PPh$_3$ groups have been replaced by methyl (Me) groups for computational convenience.

Also the solvent influence has been included, due to the demonstrated fundamental role in influencing thermodynamic and kinetic parameters in metal complex reactivity [32].

Thus, the energies reported in this work are all calculated in water represented by a polarizable continuum model (PCM) [33].

2.8. Cytotoxicity Assays

Cell Lines: U87 cells from human glioblastoma and MCF-7 cells from breast carcinoma were grown in Dulbecco's modified Eagle's medium (DMEM, Euroclone). The complete culture medium was supplemented with 10% heat-inactivated fetal bovine serum (Euroclone), streptomycin (0.2 mg mL^{-1}), and penicillin (200 IU mL^{-1}). For U87 cells the complete medium was added with 1% of non-essential amino acids. Cells were incubated at 37 °C and 5% CO_2 in a humidified incubator. The cytotoxicity assays were performed as previously described [34]. Briefly, U87 cells from human glioblastoma and MCF-7 cells from breast carcinoma were exposed to tested compounds for a period of 72 h. All tested compounds were dissolved in dmso prior to their dilution with complete cell culture medium to the predetermined experimental concentrations (seven concentrations ranging from 0.10 to 200 μM). In all experiments the percentage of dmso never exceeded 1%. Cytotoxicity (IC_{50}) values for the tested compounds were determined using the metabolic reduction of the soluble 3-(4,5-dimethylthiazol-2-yl)-2,5-diphenyltetrazolium bromide (MTT) by a mitochondrial enzyme of cultured cells into an insoluble colored formazan product. In particular, cells were seeded at a density of about 5,000 cells/well in a 96 well plate and incubated at 37 °C for 72 h in the presence and absence of the tested compounds. Untreated cells were used as positive control. Then, 10 μL of 5 mg mL^{-1} MTT solution was added to each well and the plates were incubated for additional 3 h at 37 °C. Next, cells were lysed by the addition of 150 μL of 50% (v/v) dmso and 50% (v/v) ethanol solution, and the absorbance of each individual well was measured using a microplate reader at 570 nm (Wallac Victor3, 1420 Multilabel Counter, Perkin-Elmer). The reported values are the average of triplicate measurements performed in three separate experiments.

3. Results and Discussion

3.1 Synthesis and characterization of platinum polyphenolate complexes.

The synthesis of the platinum polyphenolate complexes was achieved by reaction of *cis*-$[PtCl_2(PPh_3)_2]$ with deprotonated forms of the selected biologically active natural polyphenols in dichloromethane/ethanol [35]. The coordination of an alcoholic oxygen atom (hard donor) to platinum (soft acid) is thermodynamically disfavored and occurs when it is supported by an additional driving force, like for example the precipitation of an insoluble side product. In our case, insoluble KCl was recovered at the end of the reactions.

The reaction between *cis*-$[PtCl_2(PPh_3)_2]$ and quercetin leading to *cis*-$[Pt(PPh_3)_2(que)]$ (**1**, que = dianion of quercetin) is depicted in Scheme 4. The target complex was obtained in high yield and ca. 95% purity by slowly adding ethanolic KOH to a dichloromethane solution of *cis*-$PtCl_2(PPh_3)_2$. The presence of ca. 5% impurities, which we were not able to separate from the major product, prevented the use of complex **1** in cytotoxic essays. The formation of side-products in the synthesis of **1** is probably due to the presence of several coordination sites in quercetin [36]. In fact, beside metal complexes whereby quercetin is bonded via $C^{3'}$–O and $C^{4'}$–O [37] as in **1**, metal(II) complexes of quercetin bonded through the keto group (C^4=O) and the C^3–O oxygen atom are known [14a,38] and, in principle, also C^7–O bonded metal complexes may form.

When we tried to obtain **1** by adding an ethanolic solution of the pre-formed salt of quercetin to a solution of *cis*-$[PtCl_2(PPh_3)_2]$, the reaction was even less selective and several platinum compounds formed, as shown by ^{31}P NMR analysis.

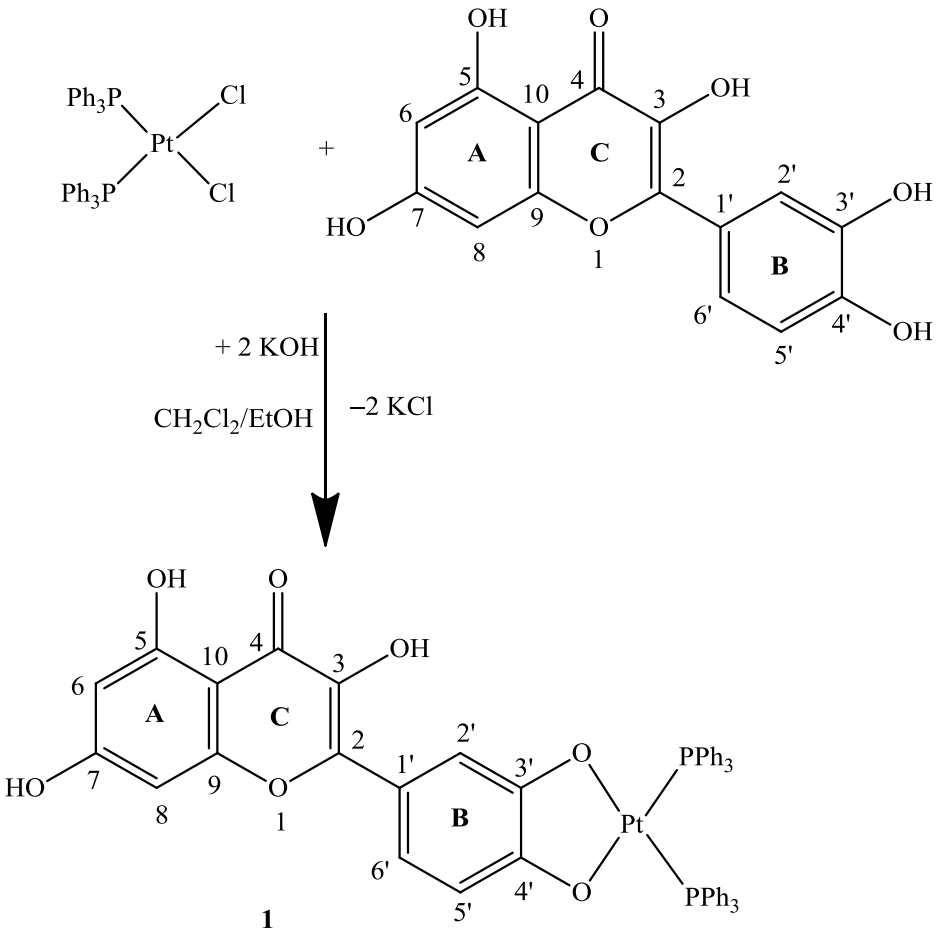

1

Scheme 4. Synthesis of *cis*-[Pt(PPh_3)$_2$(que)] (que = dianion of quercetin) (**1**).

The formula proposed for **1** was confirmed by HR ESI-MS analysis. The ESI-MS spectrogram in negative mode of a diluted acetonitrile solution of **1** showed an intense peak at *m/z* 1018.1678, whose isotope pattern is perfectly superimposable to that calculated for the anion $[C_{51}H_{37}O_7P_2Pt]^-$ (corresponding to [**1**-H]$^-$), obtained by deprotonation of an hydroxyl group under analysis conditions (Figure 1).

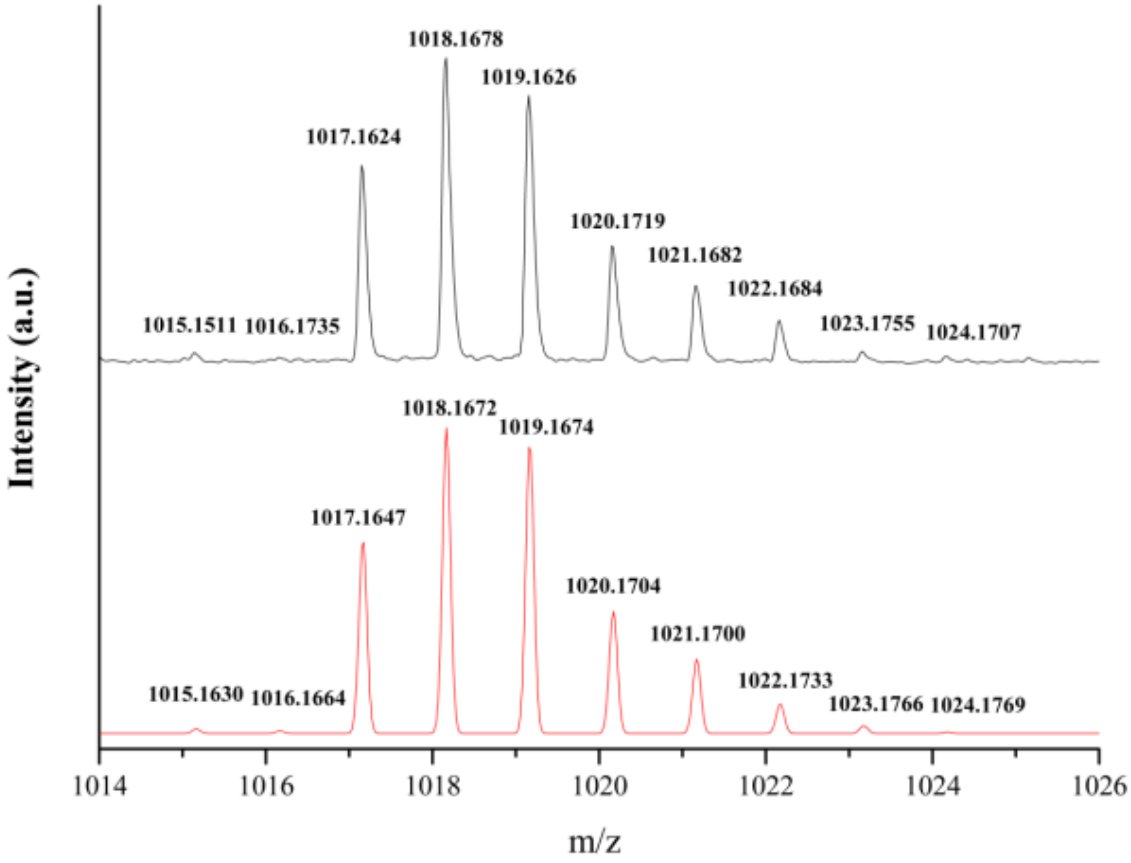

Figure 1. Experimental (top) and calculated (bottom) HRMS-spectra of **1** showing the ion [**1** – H]$^{-}$. The error between the calculated and observed isotopic patterns is 3.4 ppm.

The $^{31}P\{^{1}H\}$ NMR spectrum of **1** in dmso-d_6 showed two mutually coupled doublets ($^{2}J_{P,P}$ = 23 Hz) flanked by ^{195}Pt satellites at δ 9.6 ($^{1}J_{Pt,P}$ = 3565 Hz) and δ 8.3 ($^{1}J_{Pt,P}$ = 3600 Hz). The ^{31}P-^{31}P coupling constant indicates a structure in which the PPh_3 groups are mutually *cis*, while the direct ^{31}P-^{195}Pt coupling constant values are compatible with phosphane groups in *trans* position to an oxygen atom [37]. The $^{13}C\{^{1}H\}$ NMR spectrum of complex **1** showed a *ca*. 20 ppm downfield shift with respect to the free ligand of the carbon signals which are close to the coordination sites. In fact, the resonance of C$^{3'}$ and C$^{4'}$ signals were found (by means of ^{1}H–^{13}C HMBC and ^{1}H–^{13}C HSQC experiments, Figures S5 and S6) at δ 166.6 and δ 163.4, respectively, with those of free quercetin

falling at δ 143.6 and δ 145.0, respectively (Table 2). All ^{1}H NMR signals were unambiguously assigned by means of 1D and 2D NMR experiments and are reported in Table 3. The signal of $C^5O\mathit{H}$ ($\Delta\nu_{1/2}$ = 2 Hz) is much sharper than those of $C^3O\mathit{H}$ ($\Delta\nu_{1/2}$ = 12 Hz) and C^7OH ($\Delta\nu_{1/2}$ = 94 Hz), probably due to the formation of intramolecular $C^5OH\cdots OC^4$ hydrogen bond in solution. This is confirmed by the high value of the chemical shift found for the C^5OH proton (δ 12.64). The large broadness of the C^7OH proton signal is ascribable to the fast exchange with water. The ^{195}Pt{^{1}H} NMR spectrum of **1** consists of a doublet of doublets at δ –4062, in the region of Pt(II) phosphane complexes [37].

Table 2. ^{13}C NMR spectral data of **1**, **2** , quercetin and 3-hydroxyflavone (dmso-d_6, 298 K). Bold typeface refers to largest changes in chemical shifts observed comparing free with metal coordinated ligand.

	Complex **1**	quercetin	Complex **2**	3-hydroxyflavone
C^2	128.9	135.6	**173.6**	**139.1**
C^3	149.4	146.8	**182.6**	**145.2**
C^4	175.5	175.7	**207.0**	**173.1**
C^5	161	160.6	125.5	124.8
C^6	98.5	98.1	128.9	124.5
C^7	163.8	163.8	134.3	133.7
C^8	93.6	93.3	118.3	118.4
C^9	156.3	156.1	155.2	154.6

C^{10}	103.2	103	121.8	121.2
$C^{1'}$	118.4	121.9	131.8	131.3
$C^{2'}$	114.1	115.1	128.2	127.6
$C^{3'}$	**166.6**	**147.6**	128.4	128.6
$C^{4'}$	**163.4**	**145.0**	129.1	129.6
$C^{5'}$	115.1	115.5	128.4	128.6
$C^{6'}$	118.1	119.9	128.2	127.6

Table 3. ^{1}H NMR spectral data of **1**, **2** , quercetin and 3-hydroxyflavone (dmso-d_6, 298 K).

	Complex **1**	quercetin	Complex **2**	3-hydroxyflavone
H^3	8.81	9.6	–	9.68
H^5	12.64	12.42	8.10 (d, $^3J_{H5,H6}$= 8.4 Hz)	8.16 (d, $^3J_{H5,H6}$= 8.1 Hz)
H^6	6.12 (d, $^4J_{H6,H8}$ = 2.1 Hz)	6.18 (d, $^4J_{H6,H8}$ = 2.0 Hz)	7.51 (m)	7.50 (m)
H^7	10.63	10.76	7.87 (m)	7.82 (m)
H^8	6.32 (d, $^4J_{H6,H8}$ = 2.1 Hz)	6.40 (d, $^4J_{H6,H8}$ = 2.0 Hz)	7.98 (d, $^3J_{H7,H8}$= 7.7 Hz)	7.78 (d, $^3J_{H7,H8}$= 8.0 Hz)
$H^{2'}$	7.00 (d, $^4J_{H2',H6'}$ = 2.0 Hz)	7.67 (d, $^4J_{H2',H6'}$ = 2.2 Hz)	8.24 (d, $^3J_{H2',H3'}$= 7.7 Hz)	8.26 (d, $^3J_{H2',H3'}$= 7.9 Hz)

H$^{3'}$	-	9.31	7.74 (*m*)	7.63 (*m*)
H$^{4'}$	-	9.39	7.55 (*m*)	7.54 (*m*)
H$^{5'}$	6.19 (d, $^3J_{H5',H6'}$= 8.4 Hz)	6.89 (d, $^3J_{H5',H6'}$= 8.3 Hz)	7.74 (*m*)	7.63 (*m*)
H$^{6'}$	7.25 (*m*)	7.53 (dd, 8.3 Hz, 2.2 Hz)	8.24 (d, $^3J_{H5',H6'}$= 7.7 Hz)	8.26 (d, $^3J_{H5',H6'}$= 7.9 Hz)

The IR spectrum of **1** showed broad bands at 3372-3633 cm^{-1} that can be assigned to the hydroxyl groups C^7O–H, C^5O–H and C^3O–H, along with the typical bands ascribed to the skeletal C=C (1650 and 1426 cm^{-1}) and C–O–C (1270 cm^{-1}) stretchings. All IR bands of coordinated deprotonated quercetin are only slightly shifted in comparison to those assigned to free quercetin [39]. In particular, the 1650 cm^{-1} band assigned to the C^4=O stretching (1661 cm^{-1} in free quercetin) confirms that the coordination of quercetin does not involve the oxygen atom of the carbonyl group (the 11 cm^{-1} red-shift can be due to ring deformation caused by platinum bonding to quercetin).

Complex **1** was crystallized from thf/*n*-pentane to give crystals suitable for X-ray diffraction. An ORTEP [40] drawing of the molecule is shown in Figure 2. Table 4 reports selected bond lengths and angles for **1**. The Pt atom has a distorted square-planar coordination geometry imposed by the *O,O'* chelation of quercetin. In the molecular unit of **1** the Pt atom is displaced from the mean plane passing through the basal atoms P1, P2, O5 and O2 by 3.0 Å. The Pt–P (2.25 Å) and Pt–O (2.06 Å) distances are similar to those reported for other triarylphosphane platinum(II) complexes containing chelating phenoxides [41]. Complex **1** has orthorhombic symmetry, and a large crystal cell (cell volume 11005.3 $Å^3$, volume per atom 22.6 $Å^3$). The packing in the crystal cell is dominated by the interactions among the PPh_3 rings, which arrange them in planes perpendicular to the longer *c* axis. The dianion of quercetin are instead arranged parallel to the *c* axis, spacing out the stacked PPh_3

ligands. The O8–H8 hydroxyl group and O7 give rise, also in the solid state, to an intramolecular hydrogen bond.

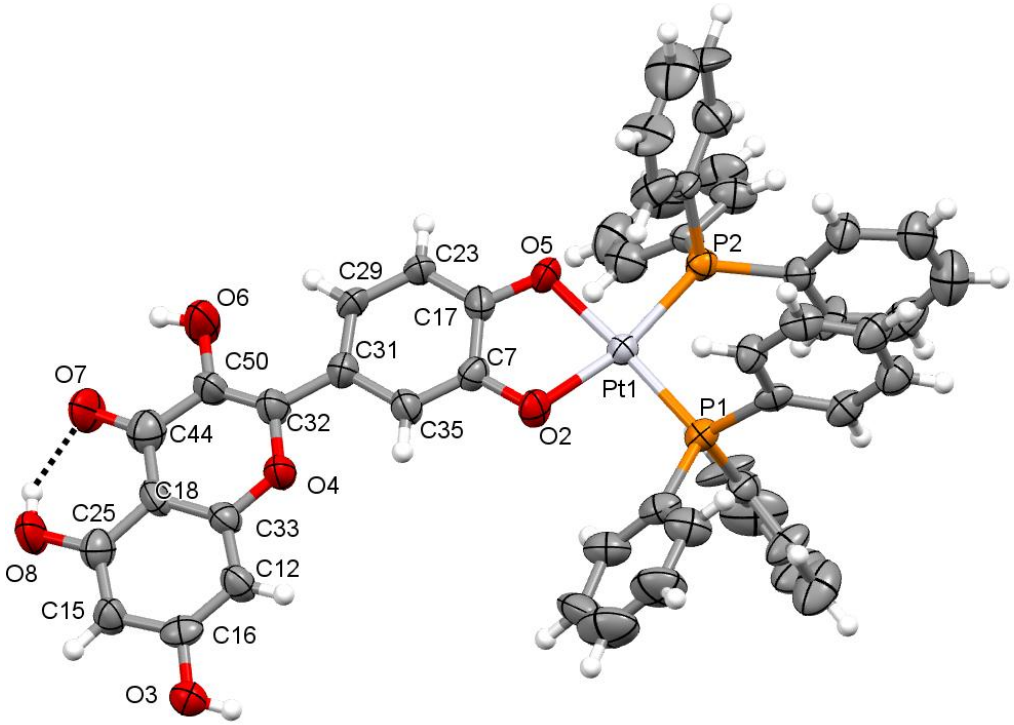

Figure 2. ORTEP [40] drawing of **1**, by using ellipsoids at 50% probability level.

Table 4. Selected bond lengths [Å] and angles [°] for complex **1**.

Bond lenghts			
Pt1-P2	2.253(2)	Pt1-O2	2.059(6)
Pt1-P1	2.249(3)	C17-O5	1.338(10)
Pt1-O5	2.055(6)	C7-O2	1.386(10)
Angles			
P1-Pt1-P2	98.67(9)	P2-Pt1-O2	167.27(19)
P2-Pt1-O5	84.78(18)	P1-Pt1-O2	93.48(18)
P1-Pt1-O5	176.51(18)	Pt1-O2-C7	108.0(57)
Pt2-O3'-C17	110.6(6)	O5-Pt1-O2	83.0(2)

When 3-hydroxyflavone reacted with *cis*-[$PtCl_2(PPh_3)_2$] under alkaline conditions, complex salt *cis*-[$Pt(PPh_3)_2$(3-Hfl)]Cl (**2**, 3-Hfl = monoanion of 3-hydroxyflavone) formed (Scheme 5), in which deprotonated 3-hydroxyflavone coordinates Pt through its O^3 and O^4 atoms. The formula proposed for **2** was indicated by HR ESI(+)-MS analysis which showed an intense peak at *m/z* 956.2021, whose isotope pattern is perfectly superimposable to that calculated for [$C_{51}H_{39}O_3P_2Pt$] corresponding to the cation *cis*-[$Pt(PPh_3)_2$(3-Hfl)]$^+$.

The ionic structure for **2** was confirmed by comparing the dmso-d_6 solution ^{31}P NMR signals of **2** before and after addition of solid $AgBF_4$. The addition of $AgBF_4$ to the yellow solution of **2** caused the immediate precipitation of AgCl, and the chemical shifts of the ^{31}P NMR signals of **2** did not change after replacement of the chloride with a poorly coordinating anion (BF_4^-), ruling out, for instance, the possibility of a neutral penta-coordinated structure [19a] for **2**.

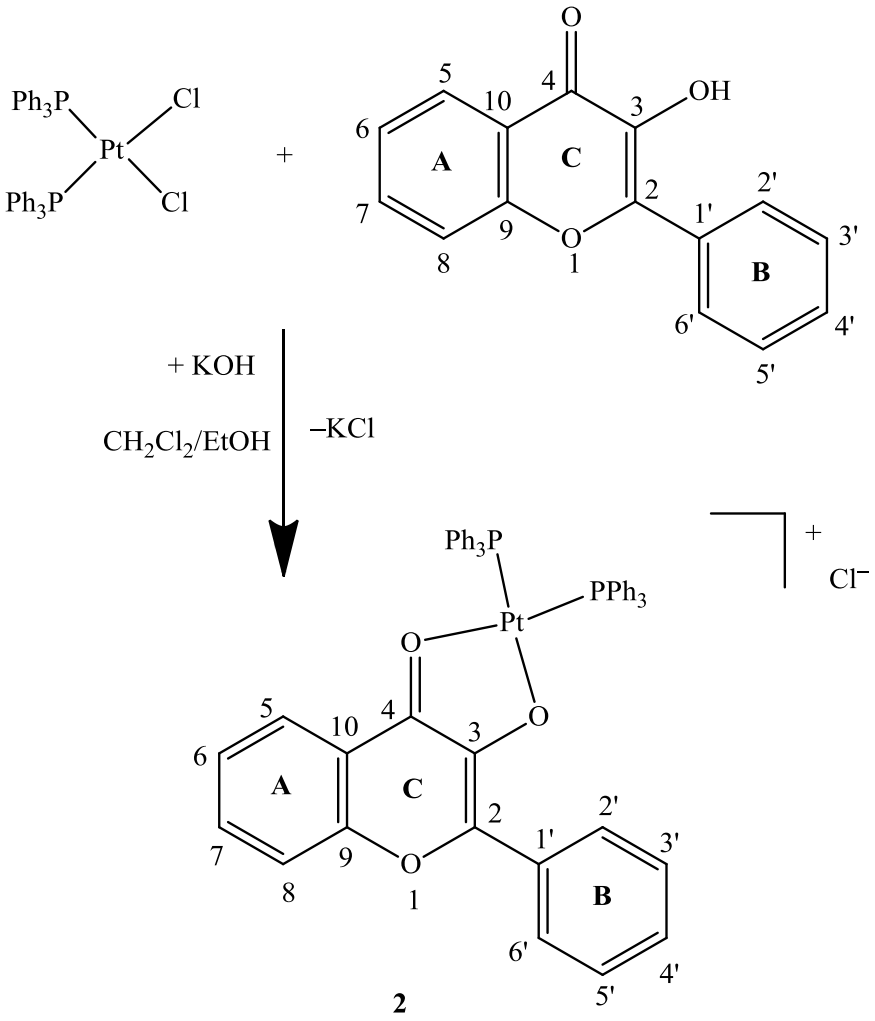

Scheme 5. Synthesis of *cis*-[Pt(PPh_3)$_2$(3-Hfl)]Cl (3-Hfl = monoanion of 3-hydroxyflavone) (**2**).

^{1}H, ^{31}P and ^{195}Pt NMR features of **2** (Table 3 and Experimental Section) are consistent with the structure proposed in Scheme 5. As for complex **1**, the ^{13}C{^{1}H} NMR spectrum of **2** showed a significant downfield shift of the carbon signals close to the coordination site, passing from δ 173.1 (C^4), δ 145.2 (C^3) and δ 139.1 (C^2) for free 3-hydroxyflavone, to δ 207.2 (C^4); δ 173.4 (C^3) and δ 154.0 (C^2) for complex **2** (Table 2). On the contrary, the ^{13}C NMR chemical shift values belonging to nuclei of A- and B-rings were very similar to the ones reported for free 3-hydroxyflavone [42]. The IR spectrum of **2** exhibited a strong sharp peak at 1613 cm^{-1} which can be assigned to the coordinated carbonyl group, while no absorptions were observed in the O–H stretching region. The ca. 50 cm^{-1} red shift of the carbonyl band observed with respect to free 3-

hydroxyflavone [36a] indicates that the metal coordination involves the oxygen atom of the carbonyl group.

Single crystals of **2** obtained by slow diffusion of *n*-pentane into the thf reaction solution were submitted to XRD analysis, but were not of sufficient quality to warrant a complete X-ray structure determination. Nonetheless, the collected data confirmed unambiguously for **2** the atom connectivity shown in Scheme 5, with the chlorine atom, whose refined occupancy was 0.45, placed in the same plane of the monoanion of 3-hydroxyflavone unit and far away from the coordination sphere of the platinum center. Three additional molecules were found in the elementary cell (*vide infra*), due to photodegradation processes.

Complex **3** was synthesized by reacting ethyl gallate with *cis*-$[PtCl_2(PPh_3)_2]$ under alkaline conditions (Scheme 6). The formula proposed for **3** was confirmed by HR ESI-MS analysis. The ESI-MS spectrogram in positive mode of **3** showed an intense peak at *m/z* 916.1845, whose isotope pattern is perfectly superimposable to that calculated for the radical cation $[C_{45}H_{38}O_5P_2Pt]^+$ (corresponding to $[\mathbf{3}]^+$).

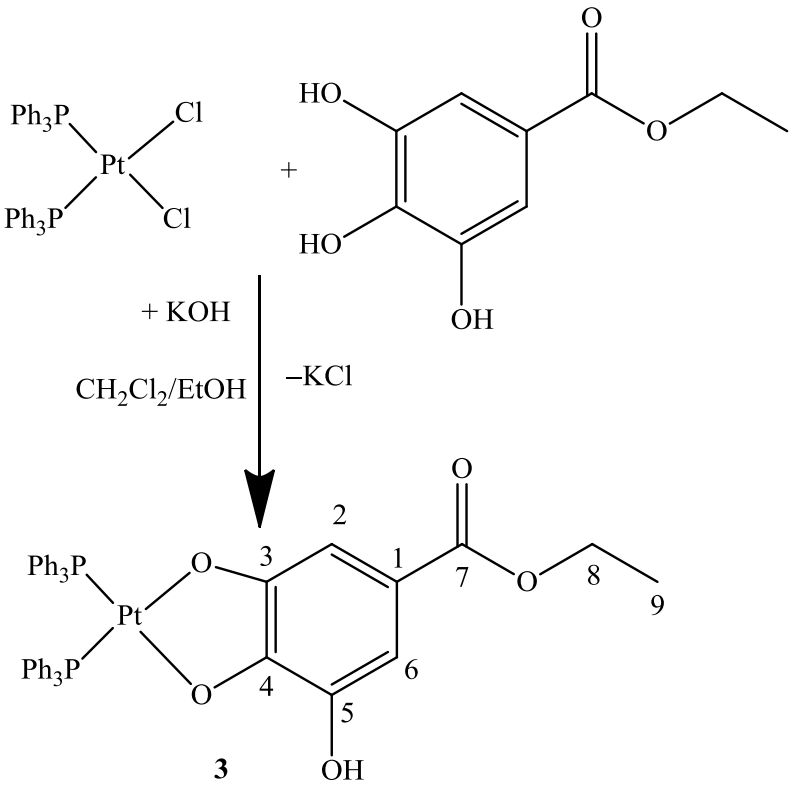

Scheme 6. Synthesis of *cis*-[Pt(PPh_3)$_2$(etga)] (etga = dianion of ethyl gallate) (**3**).

The $^{31}P\{^1H\}$ NMR spectrum of **3** in dmso-d_6 showed the expected doublets at δ 11.2 ($^1J_{Pt,P}$ = 3552 Hz) and δ 6.4 ($^1J_{Pt,P}$ 3660 Hz), while the $^{195}Pt\{^1H\}$ NMR spectrum showed a pseudo-triplet at δ –4400. The C^5-OH proton of **3** (δ 5.60) was significantly shielded respect to the free ligand (δ 9.30), presumably due to the weakening of the hydrogen bond system caused by Pt coordination. The $^{13}C\{^1H\}$ NMR spectrum confirmed the coordination of the C^3-O and C^4-O phenoxides onto Pt. In fact, C^3 and C^4 signals of the coordinated ethyl gallate were found at δ 163.1 and δ 154.6, ca. 18 ppm down-field shifted respect to the free ligand (δ 145.6 for C^3 and δ 138.3 for C^4).

Slow diffusion of *n*-pentane into a thf solution of **3** afforded crystals suitable for XRD analysis. An ORTEP [40] drawing of **3** is shown in Figure 3, while relevant bond lengths and angles are collected in Table 5. The Pt atom adopts an almost square-planar coordination geometry imposed by the *O,O'* chelation of the dianion of ethyl gallate, as well as by the crystal packing on the PPh_3

ligands. In the elementary cell, ethyl gallate moieties are all aligned in the (113) plane. Deviation from planarity of the PtP2O2 plane was observed, as measured by the improper dihedral angle value (3.2°), being the plane of the two P atoms rotated with respect to the plane of the ethyl gallate molecule.

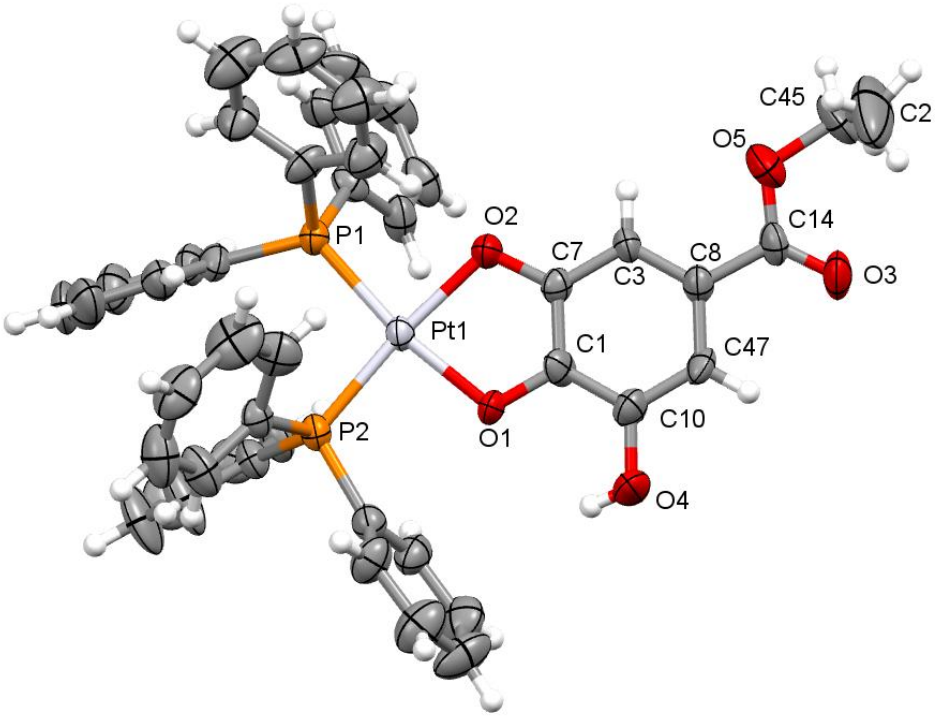

Figure 3. ORTEP [40] drawing of **3** by using ellipsoids at 50% probability level.

Table 5. Selected bond lengths [Å] and angles [°] for complex **3**.

Bond lenghts			
Pt1-P1	2.261(3)	Pt1-O1	2.028(7)
Pt1-P2	2.260(3)	C7-O2	1.346(13)
Pt1-O2	2.053(7)	C1-O1	1.357(13)
Angles			
P1-Pt1-P2	99.17(10)	P1-Pt1-O1	169.9(2)
P1-Pt1-O2	87.6(2)	P2-Pt1-O1	90.4(2)
P2-Pt1-O2	172.3(2)	Pt1-O2-C7	109.6(6)

Pt1-O1-C1	110.3(6)	O1-Pt1-O2	83.1(3)

*3.2. Photo degradation of **2** under aerobic conditions*

The photo degradation of 3-hydroxyflavone to 3-hydroxy-3-phenyl-1,2-indandione (**4**, Scheme 7) [43] is a well-known phenomenon, which has attracted the interest of the academic community [43,44]. In fact, the photo degradation of 3-hydroxyflavone affects both its biological and antioxidant activities [45] as well as its peculiar photochemical properties [46].

Conrard and coworkers reported that Zn(II) and Pb(II) 3-hydroxyflavonate complexes decompose when exposed to daylight affording **4** under both aerobic and anaerobic conditions, thus indicating that the coordination to the metal center does not influence the decomposition pathway [47].

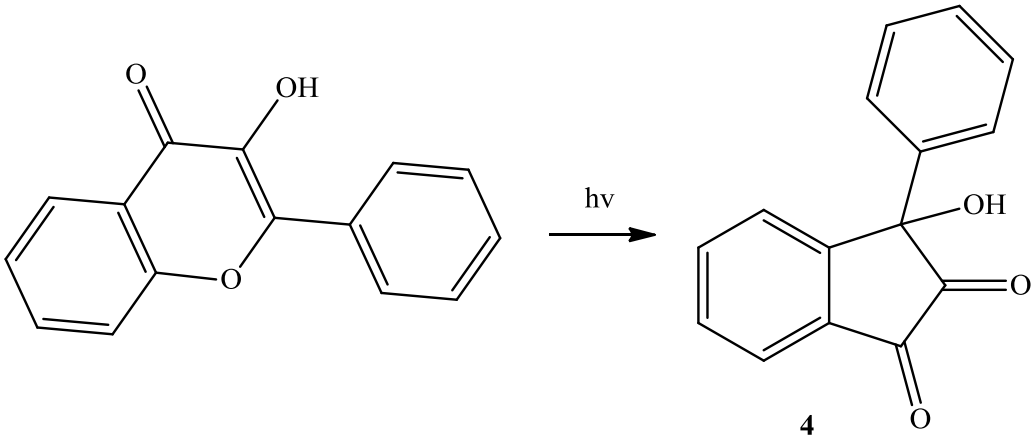

Scheme 7. Photo degradation of 3-hydroxyflavone in the absence of metal ions.

On the contrary, Berreau and coworkers reported that Pb(II), Zn(II), Ru(II) and other divalent metal flavonolate complexes undergo oxidative photochemical degradation with loss of CO [48] and formation of *O*-benzoyl salicylate complexes under aerobic conditions, and can act as catalysts for the photoinduced oxidative ring opening of 3-hydroxyflavone to give O-benzoyl salicylic acid (**5**)

[49]. A similar behaviour was observed by Speier and coworkers for Cu(II) flavonolate complexes under aerobic and thermal conditions [50].

In our case, we observed an oxidative photo degradation of **2** under aerobic conditions. In fact, when a dmso-d_6 solution of **2** was left standing under air in the daylight for five days, a new compound formed in ca. 10 % yield, which was characterized (NMR and GC-MS) as *O*-benzoyl salicylic acid (**5**). This compound was not observed when a similar solution of **2** was left standing for ten days either in the dark and/or in the absence of dioxygen.

In addition, as previously mentioned, XRD analyses of crystals obtained by a slow diffusion of *n*-pentane/thf solution of **2** kept one month under air in daylight showed in the elementary cell additional atoms beside those belonging to complex **2**. They have been placed to interpret clear peaks emerging in the difference Fourier electron density, and allowed to improve significantly the refinement of the whole structure. Such atoms are grouped to form three additional molecules: a salicylic acid, a thf (crystallization solvent) molecule and a fragment, which was tentatively identified as benzoic acid, but whose low resolution prevented a conclusive assignment.

On the basis of these observations, the photo degradation pathway followed by **2** should resemble the one already reported by Berreau and coworkers for Ru(II) flavonolate complexes [48] (Scheme 8). Aerobic oxidation of **2** would result in a carbonyl Pt complex bonded to the anion of *O*-benzoyl salicylic acid. This intermediate can decompose, in the presence of adventitious water, to give **5** plus unidentified Pt species. The formation of salycilic acid and benzoic acid during slow crystallization of **2** in *n*-pentane/thf might then derive from hydrolysis of **5**.

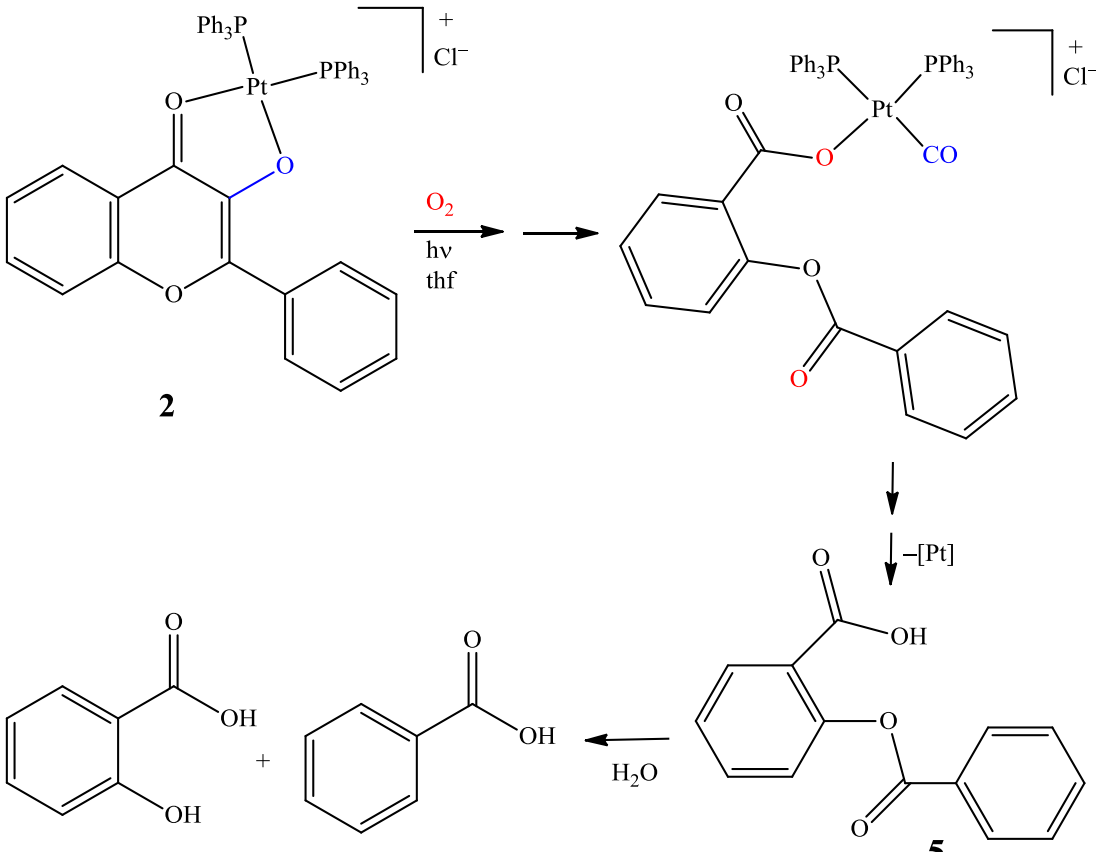

Scheme 8. Plausible pathway for the aerobic photo degradation of **2**. [Pt] represents undefined Pt species.

3.3.*DFT calculations*

On the basis of a large number of experimental data, it is widely accepted that the hydrolysis of platinum(II) anticancer complexes is a bimolecular nucleophilic substitution (S_N2) which is the rate-determining step of the process leading to the formation of the adduct with DNA nucleobases [**Error! Bookmark not defined.**]. In particular, for cisplatin the mono-aquo species is believed to be the key player, since it coordinates to the N7 atom of a guanine base in DNA producing a monofunctional adduct [**Error! Bookmark not defined.**,51]. Once coordinated, the second chloride is released and platinum binds a second base producing the crosslink, which distorts DNA [**Error! Bookmark not defined.**]. Due to their importance, the hydrolysis reactions of platinum complexes have been studied by means of a variety of theoretical methods in the last decade [21]. In

our case, the activation energies for the hydrolysis reactions of complexes **2** and **3** have been calculated because they could be correlated to their potential synergic cytotoxicity, since polyphenols are released in solution.

The first hydrolysis leads to the ring-opening process, with the 3-Hfl and etga derivatives remaining mono-coordinated to the metal ion center. The second hydrolysis (second step) leads to the complete release of 3-Hfl and etga (Scheme 9).

For comparison purposes, we considered also the hydrolysis of *cis*-[$Pt(PMe_3)_2(Cl_2)$] (see Supplementary Information), and that of cisplatin [**Error! Bookmark not defined.**a].

3.3.1. Hydrolysis reaction for cis-[$Pt(PMe_3)_2$(etga)].

The optimized geometry parameters of the model complex *cis*-[$Pt(PMe_3)_2$(etga)] (Table S1) are in excellent agreement with the experimental ones found for complex **3** (Table 5), thus confirming the reliability of the computational protocol used. In Figure 4 the structures of reactants (R), products (P) and transition states (TS) are shown for both reaction paths (Scheme 9a) while the energy profiles are shown in Figure 5. The energy (E) values are referred to the separated reactants (R) rather than reactant adducts (RA) (Figure 4), since it is wide accepted that at the beginning of the reaction, the water molecule in the second coordination shell of the metal is possible only in vacuum, but it seems an artifact in solution [52]. Relevant bond distances of all optimized complexes are reported in Table S2. The energy values corresponding to Figure 5 are reported in Table S3.

The detachment of the etga ligand in the first hydrolysis can occur in two different ways (Scheme 9a): by rupture of the bond that involves the oxygen in α position to the OH group (O1 path) or by breaking the other Pt-O bond (O2 path). Both O1 and O2 paths (Figure 4a) showed a proton transfer from the incoming water molecule to the closer oxygen of the ligand (OL). This result has been previously reported also for the hydrolysis of other platinum drugs under neutral conditions [**Error! Bookmark not defined.**c,**Error! Bookmark not defined.**d]. Mono- and di-hydroxo complexes

should form under physiological conditions, although it has been reported that the local pH in the vicinity of macromolecules could be different from the physiological one [53].

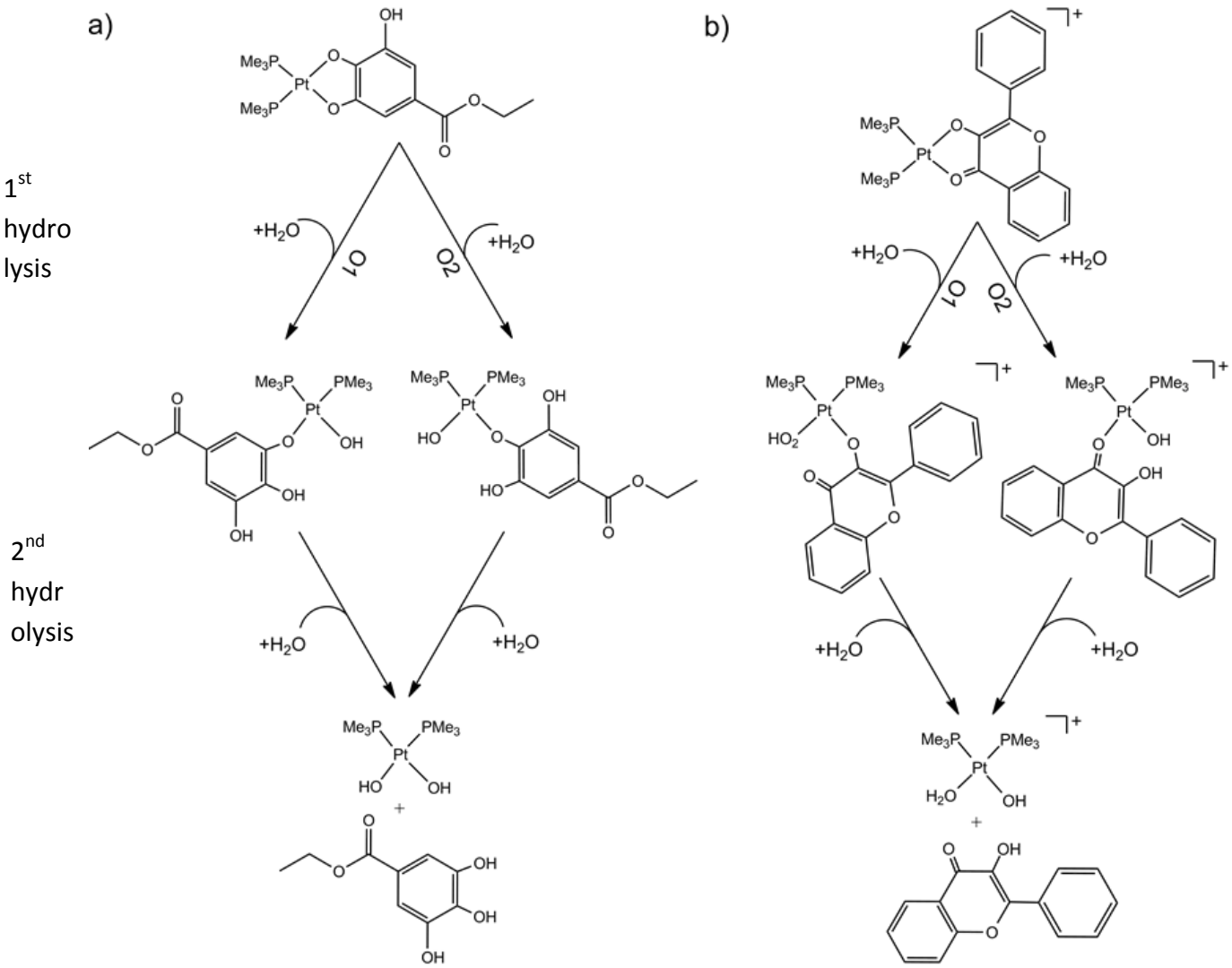

Scheme 9. Hydrolysis reactions for: a) *cis*-[Pt(PMe$_3$)$_2$(etga)] and b) *cis*-Pt[(PMe$_3$)$_2$(3-Hfl)]$^+$

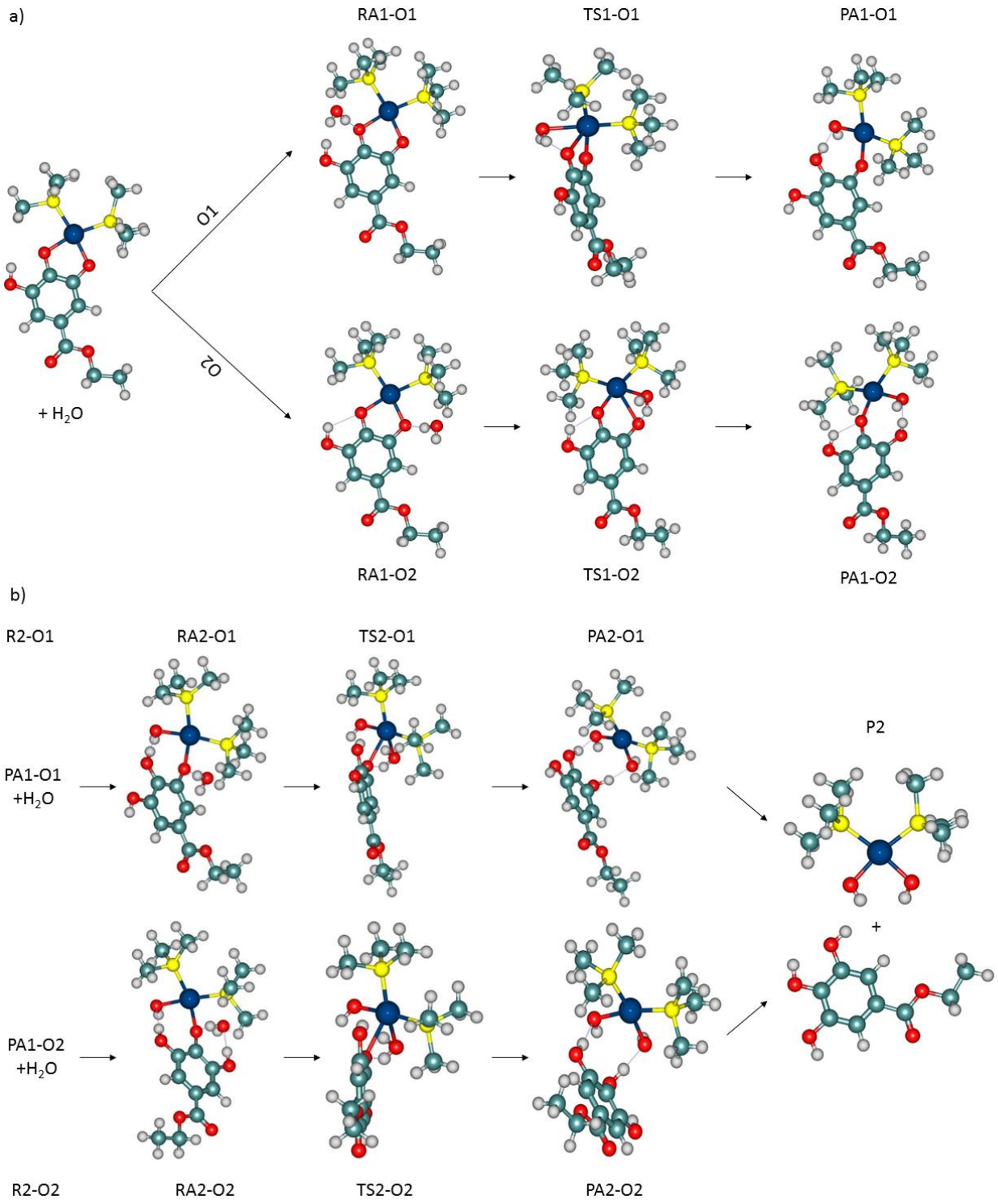

Figure 4. Optimized structures for the hydrolysis reaction of *cis*-[Pt(PMe_3)$_2$(etga)]. a) first step; b) second step.

The energy profiles for the first step of the hydrolysis indicate that the formation of the reactant adducts (RA1-O1 and RA1-O2) is energetically favored (Figure 5a and Table S4).

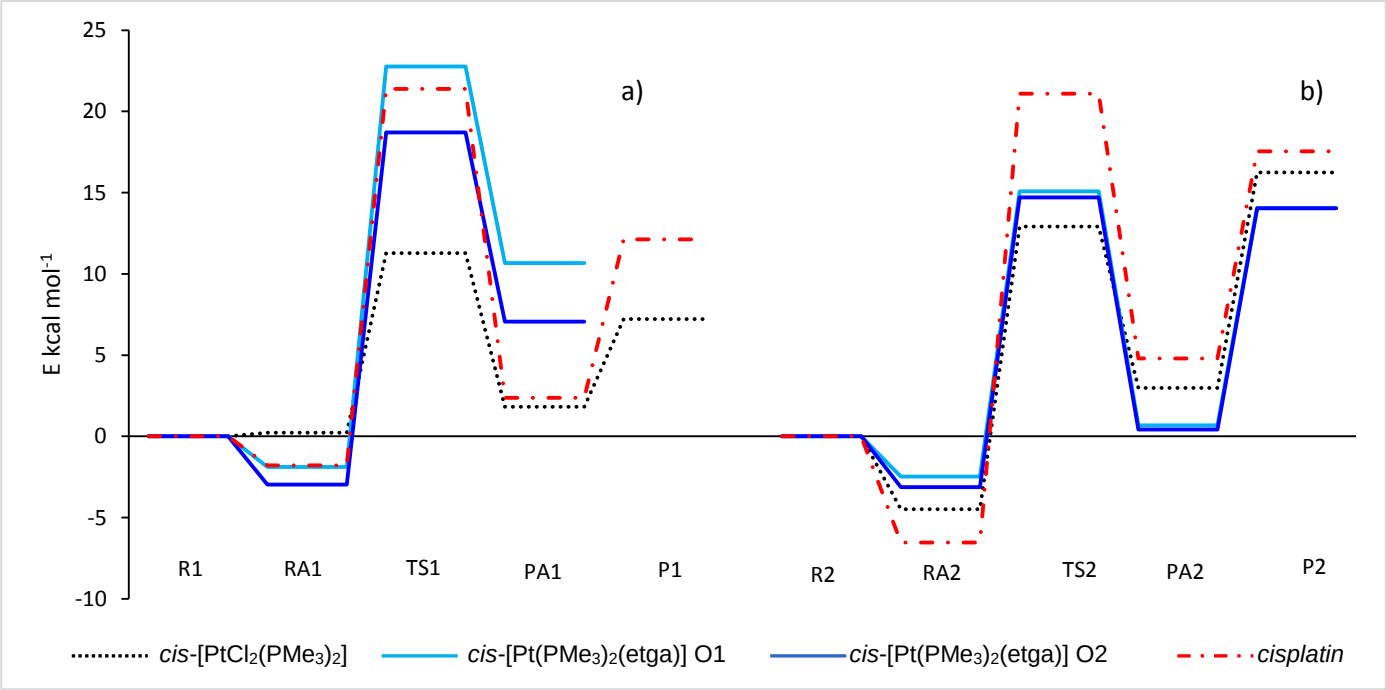

Figure 5. Activation energy profiles of: a) the first and b) the second step of the hydrolysis reaction of *cis*-[Pt(PMe$_3$)$_2$(etga)] (both O1 and O2 paths), *cis*-[PtCl$_2$(PMe$_3$)$_2$] and cisplatin in PCM water. The energy values for cisplatin are taken from ref. [**Error! Bookmark not defined.**a].

Both transition states TS1-O1 and TS1-O2 have a penta-coordinated structure, with imaginary frequencies of 99.7 cm^{-1} for TS1-O1 and 157.8 cm^{-1} for TS1-O2 corresponding to the rupture of the platinum-ligand bond (Pt-OL) and the simultaneous formation of a new bond between the metal and a water molecule. The activation energies ($E_a = E_{transition\ state} - E_{reactants}$) for the two paths are rather different: for the O1 path E_a = 22.8 kcal mol^{-1}, while the O2 path shows a E_a = 18.7 kcal mol^{-1} (Table S4). According to these results, the release of ethyl gallate by the opening of the Pt-O2 bond is kinetically preferred. Furthermore, O2 pathway leads to the most stable product [ΔE = E(PA1-O1)–E(PA1-O2) = 3.6 kcal mol^{-1}]. This difference could be due to the formation of *two* hydrogen bonds in the case of PA1-O2 with respect to PA1-O1 where only *one* hydrogen bond is possible (Figure 4a).

The transition states in the second hydrolysis have a penta-coordinated structure with imaginary frequencies of 103.9 cm^{-1} for TS2-O1 and 101.7 cm^{-1} for TS2-O2 (Figure 4b) corresponding to the

simultaneous rupture of the bond between platinum and the ligand (Pt-OL) and the formation of the metal-water bond. The calculated profiles (Figure 5b) show that the two reaction paths have comparable activation energy [$\Delta E_a = E_a$(TS2-O1)- E_a(TS2-O2) = 0.4 kcal mol^{-1}, Table S4]. Also the final products (P2) have almost the same energy of TS2-O1 and TS2-O2 (Table S3).

As shown in Figure 5 and Table S4, the first hydrolysis step has a higher activation energy with respect to the second step, irrespective of the ring opening order, thus the first hydrolysis process is the rate determining step (RDS) of the whole reaction leading to the release of ethyl gallate in solution.

Regarding the first hydrolysis (Figure 5a), by comparing the energy profiles of *cis*-[Pt(PMe_3)$_2$(etga)] with those of the highly cytotoxic cisplatin, it appears that the E_a in O2 path is lower than the cisplatin one ($\Delta E_a = E_a$(TS1-O2) – E_a(cisplatin) = –2.7 kcal mol^{-1}); on the contrary the E_a in O1 path is higher than the one calculated for cisplatin (ΔE_a = +1.4 kcal mol^{-1}) (Figure 5a and Table S4). For the second hydrolysis step, E_a values for both O1 and O2 paths are much lower than cisplatin one (ΔE_a = –6 kcal mol^{-1} for O1 path and ΔE_a = –6.4 kcal mol^{-1} for O2 path) (Figure 5b and Table S4). The obtained results suggest that *cis*-[Pt(PMe_3)$_2$(etga)] smoothly leads to a mono-hydroxo complex with etga mono-coordinated to the metal, which promptly reacts with another water molecule giving the di-hydroxo species. The mono-hydroxo and di-hydroxo species are considered poorly reactive for DNA coordination, thus their formation can limit the efficacy of a platinum metallodrug [54]. Furthermore, the low activation energy barriers of the second step and the consequent high hydrolysis reaction rate might make this complex subject to fast degradation, causing potentially poor pharmacological activity [55]. In fact, the E_a values (11.3 and 12.9 kcal mol^{-1} for the first and second hydrolysis process, respectively) calculated for *cis*-[$PtCl_2(PMe_3)_2$] (taken as a model for the biologically inactive (*vide infra*) *cis*-[$PtCl_2(PPh_3)_2$]) are much lower than the hydrolysis activation energies calculated for both *cis*-[Pt(PMe_3)$_2$(etga)] and cisplatin (Figure 5

and Table S4). In conclusion, on the basis of DFT calculations, complex **3** should not be expected highly cytotoxic.

3.3.2. Hydrolysis reaction for cis-[Pt(PMe$_3$)$_2$(3-Hfl)]$^+$.

In Figures 6 the optimized structures of the complexes involved in the hydrolysis of *cis*-[Pt(PMe$_3$)$_2$(3-Hfl)]$^+$ are displayed, with relevant bond distances reported in Tables S4 and S5.

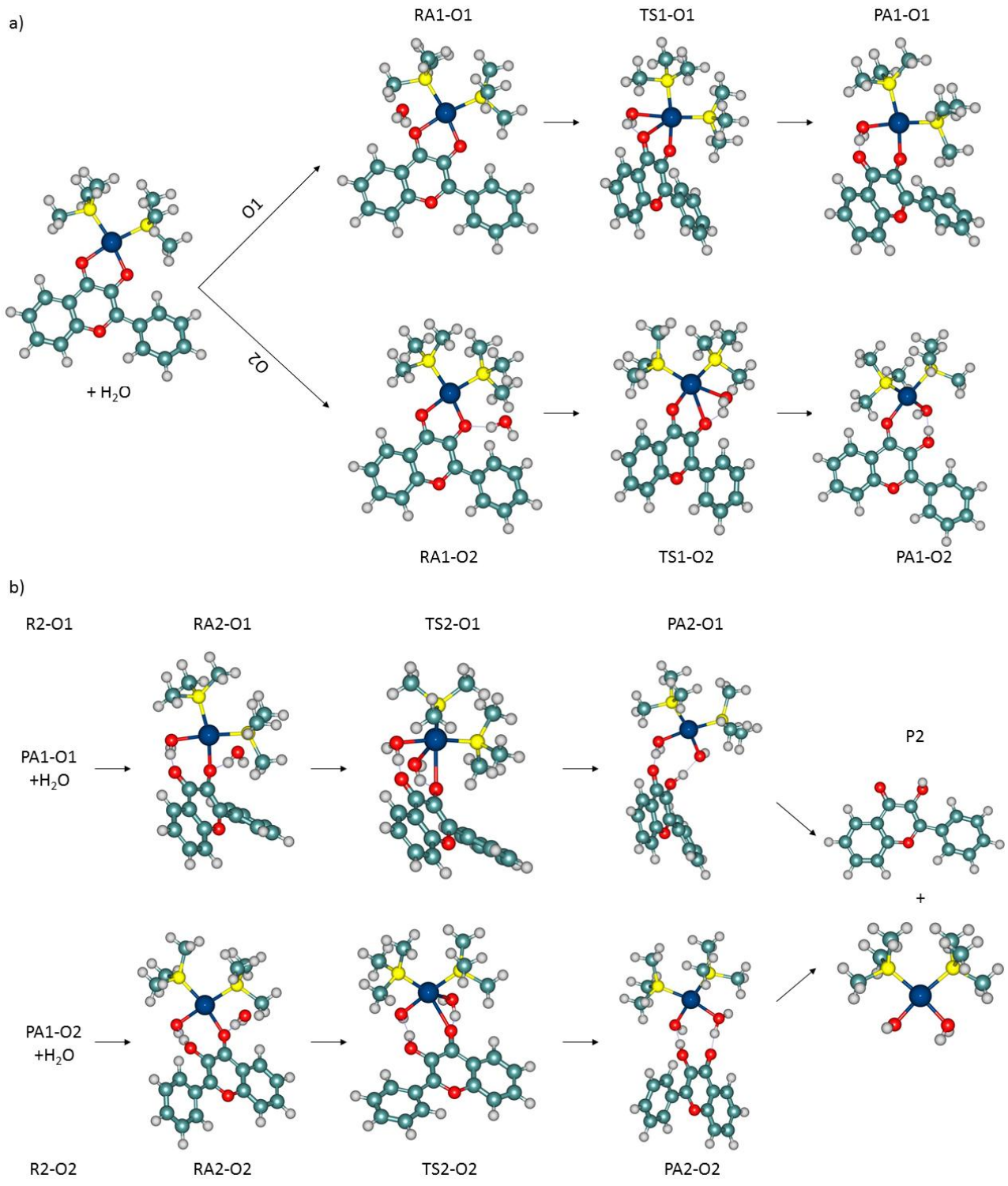

Figure 6. Optimized structures for the hydrolysis reaction of *cis*-$[Pt(PMe_3)_2(3\text{-Hfl})]^+$. a) first step; b) second step.

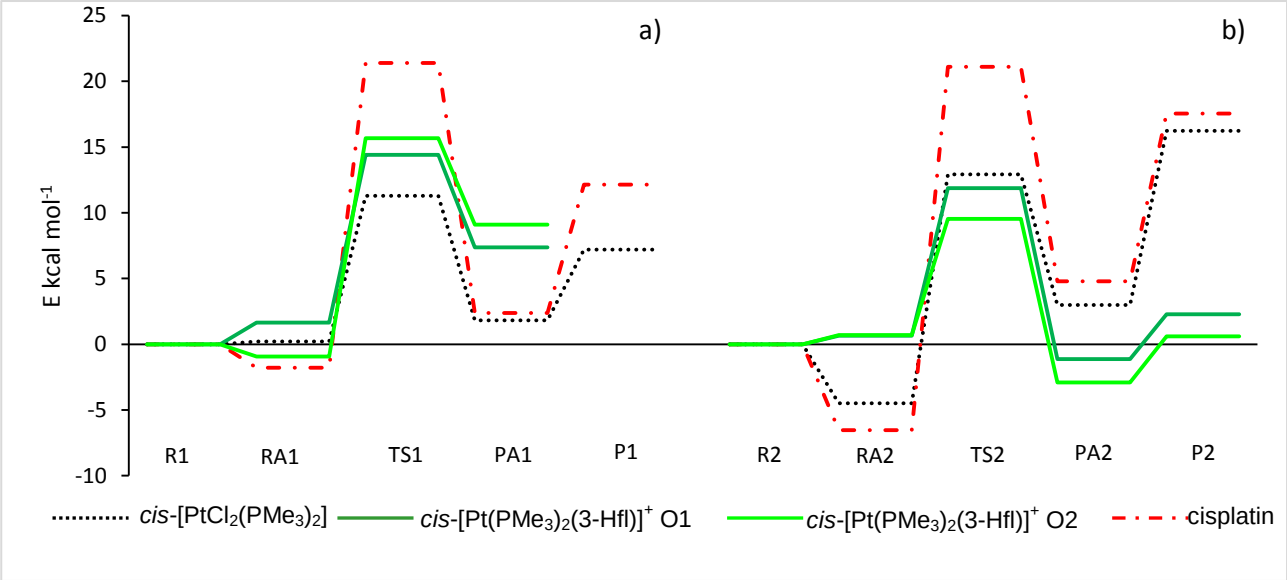

Figure 7. Activation energy profiles of: a) the first and b) the second step of the hydrolysis reaction of *cis*-$[Pt(PMe_3)_2(3\text{-Hfl})]^+$ (both O1 and O2 paths), *cis*-$[PtCl_2(PMe_3)_2]$ and cisplatin in PCM water. The energy values for cisplatin are taken from ref. [**Error! Bookmark not defined.**a].

The energy (E) profiles for the reactions in Scheme 9b are shown in Figure 7 (values in Table S3). The formation of the intermediate RA1-O2 is slightly energetically favored, while RA1-O1 formation energy is slightly positive. Also in this case, the transition states of both O1 and O2 paths have a penta-coordinated structure with imaginary frequencies of 87 cm^{-1} for TS-O1 and 78 cm^{-1} for TS-O2. The calculated E_a values are 14.4 kcal mol^{-1} and 15.7 kcal mol^{-1} for O1 and O2 path, respectively. The O1 opening produces the mono-aqua derivative, while in the O2 path a proton transfer leading to the mono-hydroxo complex occurs. Also the PA1-O1 is more stable than PA1-O2 [ΔE = E(PA1-O1)–E(PA1O2) = –1.8 kcal mol^{-1}, Table S4]. In conclusion, in the first hydrolysis step the O1 path, leading to a monoaqua Pt complex, should be more favored than the O2 one (which leads to a monohydroxo Pt complex).

In the second hydrolysis step (Figure 7b), transition states with a penta-coordinated Pt geometry are obtained (imaginary frequencies: 89 cm^{-1} for TS2-O1 and 83 cm^{-1} for TS2-O2). The calculated E_a values are 11.9 kcal mol^{-1} and 9.5 kcal mol^{-1} for O1 and O2 path, respectively (Table S4).

Therefore, also for *cis*-$[Pt(PMe_3)_2(3\text{-Hfl})]^+$ the first hydrolysis is the rate determining step of the whole process leading to the complete release of the 3-Hfl. Furthermore, by analyzing the obtained E_a values (Figures 7b, Figures S1-2 , Table S4), it emerges that the second hydrolysis step proceeds faster for *cis*-$[Pt(PMe_3)_2(3\text{-Hfl})]^+$ (both O1 and O2 paths) than for cisplatin and *cis*-$Pt(PMe_3)_2$(egta) (Figure 6 and Table S4). On the contrary, the first hydrolysis is slower for *cis*-$[Pt(PMe_3)_2(3\text{-Hfl})]^+$ with respect to *cis*-$[PtCl_2(PMe_3)_2]$ (Figure 7a).

In the O1 path the final product shows a proton transfer from the water molecule bonded to platinum to the closer oxygen of the ligand, while in the O2 path this phenomenon does not occur. Finally, the final product of *cis*-$[Pt(PMe_3)_2(3\text{-Hfl})]^+$ hydrolysis is the monoaqua-monohydroxo complex (*cis*-$[Pt(PMe_3)_2(H_2O)(OH)]^+$, Figure 6b).

On the basis of DFT calculations, some cytotoxic synergic effect between platinum center and 3-hydroxyflavon leaving group effect might be expected for *cis*-$Pt[(PMe_3)_2(3\text{-Hfl})]^+$, because the mono-aqua platinum species formed in both first and second hydrolysis steps, could coordinate DNA [**Error! Bookmark not defined.**]. On the other hand, the theoretical hydrolysis activation energy (mainly affected by the *trans* influence of the carrier ligand), lower than cisplatin (Figure 7) could lead to fast deactivation of platinum compound and thus poorer biological activity [55].

3.4. Cytotoxicity

The antiproliferative potential of the new complexes **2** and **3** was assessed in human glioblastoma (U87) and human breast cancer (MFC-7) cells, being the first cellular line sensitive to cisplatin and the latter cisplatin resistant. Since complex **2** was found to be photosensitive (see paragraph *3.2*), cytotoxicity studies were carried out in the dark for all examined compounds, in order to avoid photodegradation processes. Complex **1** was not taken into consideration, due to the difficulty in separating it from the side-products formed in minor amounts during its synthesis.

For comparison purposes, the cytotoxicity of 3-hydroxyflavone, ethyl gallate and *cis*-$[PtCl_2(PPh_3)_2]$ was evaluated under the same experimental conditions employed for the other metal complexes.

Cellular viability was determined by colorimetric MTT assay [MTT = 3-(4,5-dimethylthiazol-2-yl)-2,5-diphenyltetrazolium bromide]. The viability of cells in the presence of the tested compounds was compared to that observed for control cultures and the inhibition of growth (%) was calculated. The half maximal inhibitory concentration (IC_{50}) values obtained following exposure to increasing concentrations (from 0.10 to 200 μM) of the different compounds for 72 h are shown in Table 6, which reports also the relevant IC_{50} values for cisplatin taken from the literature [56].

At the tested concentrations, the Pt complexes **2** and **3** showed a different biological effect on both U87 and MCF-7 cell lines (Table 6), being **2** more cytotoxic than **3**, following the same trend observed for the relevant ligands. In fact, 3-hydroxyflavone was found more cytotoxic than ethyl gallate on the examined cell lines. This behavior confirms what predicted by DFT calculations (see previous paragraph), that is complexes **2** and **3** easily lose their natural ligands with the consequence that their cytotoxicity is mainly affected by the biological activity of their leaving groups. Theoretical studies also predicted that the platinum species (intermediates and final product) obtained from the hydrolysis of complex **3** should poorly interact with DNA: thus the cytotoxicity of complex **3** is expected to be determined by ethyl gallate only (no synergic effect). Interestingly, considering the cytotoxicity on MFC-7 cells, complex **2** is more active than the basic compounds, *i.e.* 3-hydroxyflavone and *cis*-$[PtCl_2(PPh_3)_2]$, the latter having a very negligible in vitro cytotoxicity (IC_{50} > 200 μM) for both studied cell lines. The synergism shown by **2** could be related to the formation of mono-aqua platinum species which are known to interact with DNA [**Error! Bookmark not defined.**].

Table 6. Cytotoxicity of hydroxyflavone, ethyl gallate, Pt complex **2**, Pt complex **3**, *cis*-$[PtCl_2(PPh_3)_2]$ and cisplatin toward U87 and MCF-7 cancer cell lines.

	IC_{50} (μM)	
Compound	**U87**[a]	**MCF-7**[a]
complex **2**	26.3 ± 2.1	55.2 ± 1.7
3-hydroxyflavone	27.5 ± 2.3	108.1 ± 3.5
complex **3**	123.7 ± 3.8	> 200
ethyl gallate	97.7 ± 2.6	> 200
cis-$[PtCl_2(PPh_3)_2]$	> 200	> 200
cisplatin	1.76 ± 0.22[b]	14 ± 3[c]

[a] Cells were seeded at a density of ~5000 cells per well into 96-well microliter plates. Following overnight incubation, cells were treated with a range of drug concentrations (from 0.10 to 200 μM) and incubated at 37 °C under a humidified atmosphere with 5% CO_2 for a period of 72 h. Data are the mean values ± SD of three independent experiments performed in triplicate. [b] data taken from ref [56a]. [c] data taken from ref [56b].

4. Conclusions

This article describes the synthesis and *in vitro* anticancer features of new *cis*-diphenylphosphane platinum(II) complexes bearing biologically active polyphenolate leaving group ligands. The coordination modes of deprotonated quercetin, 3-hydroxyflavone and ethylgallate to platinum(II) were determined in solution by NMR spectroscopy and in the solid state by X-ray diffraction. Biological assays carried out on complexes **2** and **3** indicate that these compounds did not show higher cytotoxicity compared to cisplatin for the considered cell lines (U87 and MCF-7). DFT calculations confirm that the studied complexes easily release their biologically active ligand in

solution, thus explaining why their observed cytotoxicity features were at least not worse than those of their natural leaving groups.

Although complexes **2** and **3** have similar *O,O'* chelate structure, there is a small difference in their natural ligand coordination mode, being the leaving group a deprotonated α-hydroxy ketone in the first complex and a double deprotonated 1,2-diol in the second one. This small difference may affect the biological activity of the new compounds.

In fact, a biological synergic effect between the ligand and the starting platinum compound was interestingly observed for complex **2** bearing 3-hydroxyflavonate, for which mono-aqua platinum species (able to coordinate DNA) smoothly form in both first and second hydrolysis steps, according to theoretical studies. However, the cytotoxicity of cisplatin is still higher than that of complex **2** one because of a too fast hydrolysis rate of the latter, due to the higher *trans* effect of the carrier ligand.

As to **3**, DFT calculations suggest that the lack of synergic cytotoxicity effect may be due either to production of relatively inert mono- and di-hydroxo complexes under physiological conditions (determined by ethyl gallate leaving group) and to a too fast hydrolysis rate (determined by carrier ligand features).

In conclusion, this study suggests that fine tuning of chemical parameters of both leaving groups and carrier ligands is a key step in designing biologically active Pt complexes. Therefore, further studies are warranted to synthesize new platinum(II) 3-hydroxoflavonate complexes bearing carrier ligands different than triarylphosphanes.

Acknowledgements

The authors thank Dr. Vito Filippo Capodiferro, Department of Pharmacy, University of Bari, Italy, for elemental analyses, Mr. Giuseppe Chita for diffraction data collection, Prof. Vito Gallo for

useful discussions and Italian MIUR (PRIN project 2010–2011 n. 2010FPTBSH, NANOMED) for financial support.

5. References

[1] B. Rosenberg, L. Van Camp, T. Crigas, *Nature*, **1965**, *205*, 698-699.

[2] a) S. Garattini, C. La Vecchia, *Eur. J. Cancer*, **2001**, *37*, 128-147; b) L.R. Ferguson, A.E. Pearson, *Mutat. Res.* **1996**, *355* , 1-12; c) D. Lebwohl, R. Canetta, *Eur. J. Cancer,* **1998,** *34*,1522-1534.

[3] N. J. Wheate, S. Walker, G. E. Craig, R. Oun, *Dalton Trans.*, **2010**, *39*, 8113–8127.

[4] a) J. B. Harborne Nature, distribution, and function of plant flavonoids. In: Plant Flavonoids in Biology and Medicine: Biochemical, Pharmacological, and Structure-Activity Relationships. Cody V, Middleton E Jr and Harborne JB (eds.), Alan R. Liss, Inc., New York, **1986**,15-24; b) J. B. Harborne and C. A. Williams, *Phytochemistry***, 2000,** *55*, 481-504.

[5] C. Kanadaswami, L.-T. Lee, P.-P. H. Lee, J.-J. Hwang, F.-C. Ke, Y.-T. Huang and M.-T. Lee, *In Vivo*, **2005** ,*19*, 895-910.

[6] H Sakagami, Y Jiang, K,Kusama, T Atsumi, T Ueha, M Toguchi, I Iwakura, K Satoh, T Fukai, T. Nomura, *Anticancer Res*, **2000***;20*, 271–277.

[7] W. Ren, Z. Qiao, H. Wang, L. Zhu, L. Zhang, *Med. Res. Rev.*, **2003,** *23*, 519–534.

[8] R.F.V. de Souza, W. F. De Giovani, *Redox Rep***., 2004**, *9*, 97-104.

[9] a) C. D., Kanakis, P. A Tarantilis, M. G. Polissiou, S. Diamantoglou, H. A. Tajmir-Riahi, *Cell Biochem. Biophys*, **2007**, *49*, 29−36; N; b) K. Janjua, A. Siddiqa, A. Yaqub, S. Sabahat, R. Qureshi, S. Haque, *Spectrochim. Acta, Part A* **2009**, *74*, 1135−1137.

[10] J. Lia, Y. Wanga, J.-C. Lei, Y. Hao, Y. Yanga, C.-X. Yangc and J.-Q. Yu, *Nat. Prod. Res*. **2014**, *28*, 683−689.

[11] Y. Wang, A. Han, E. Chen, R. K. Singh, C. O. Chichester, R. G. Moore, A. P. Singh, N. Vorsa *Int. J. Oncol*. **2015**, *46*, 1924-1934.

[12] T. J. Zwang, K. Singh, M. S. Johal, C. R. Selassie, *J. Med. Chem*, **2013**, *56*, 1491−1498.

[13] a) M. Kviecinski, K. Felipe, T. Schoenfelder, L. de Lemos Wiese, M. Rossi, E. Goncalez, J. Felicio, D. Filho, R. Pedrosa, *J. Ethnopharmacol* **2008**, *117*, 69–75; b) H. Cui, J. Yuan, X. Du, M. Wang, L. Yue, J. Liu, *Oncol. Rep.*, **2015**, *33*, 1284-1290; c) T. Kalaivani, C. Rajasekaran, and L. Mathew, *J. Food Sci.*, **2011** ,*76*, T144-T149; d) S. Mohan, K. Thiagarajan, R. Chandrasekaran, *Nat. Prod. Res*, **2015**, *29*, 366-369.

[14] a) M. Grazul, E. Budzisz, *Coord. Chem. Rev.*, **2009**, *253*, 2588–2598; b) A. Kurzwernhart, W. Kandioller, É. A. Enyedy, M. Novak, M. A. Jakupec, B. K. Keppler, C. G. Hartinger, *Dalton Trans*., **2013**, *42*, 6193-6202.

[15] J. Stawinaska, M. Ciesalak-Golonka, *Transit. Metal. Chem.*, **2001,** *26*,153-159.

[16] a) A. Medrano, S. M. Dennis, A. Alvarez-Valdés, J. Perles, T. McGregor Mason, A. G. Quiroga, *Dalton Trans*., **2015**, *44*, 3557–3562; b) M. Ravera, E. Gabano, M. Sardi, E. Monti, M. B. Gariboldi, D. Osella, *Eur. J. Inorg. Chem*, **2012**, 3441-3448; c) P. Bergamini, V. Ferretti, P. Formaglio, A. Marchi, L. Marvelli, F. Sforza, *Polyhedron* **2014**,*78*, 54–61.

[17] a) F. J. Ramos-Lima, A. G. Quiroga, B. Garcia-Serrelde, F. Blanco, A. Carnero and C. Navarro-Ranninger, *J. Med. Chem.*, **2007**, *50*, 2194–2199; b) D. Belli Dell'Amico, L. Dalla Via, A. N. Garcia-Argaez, L. Labella, F. Marchetti, S. Samaritani, *Polyhedron*, **2015**, *85*, 685-689.

[18] D. Montagner, E. Zangrando, B. Longato, *Inorg. Chem*. **2008**, *47*, 2688-2695.

[19] a) M. Frezza, Q. P. Dou, Y. Xiao, H. Samouei, M. Rashidi, F. Samari, B. Hemmateenejad, *J. Med. Chem*. **2011**, *54*, 6166–6176; b) S. Bombard, M. B. Gariboldi, E. Monti, E. Gabano, L. Gaviglio, M. Ravera, D. Osella, *J. Biol. Inorg. Chem.* **2010**, *15*, 841–850.

[20] E. R. Jamieson, S. J. Lippard, *Chem Rev* **1999**, *99*, 2467–2498.

[21] a) A. Melchior, E. Sánchez Marcos, R. R. Pappalardo, J. M. Martínez, *Theor. Chem. Acc.* **2011**, *128*, 627–638; b) A. Melchior, J. M. Martínez, R. R. Pappalardo, E. Sánchez Marcos, *J.Chem.Theor.Comp.* **2013**, *9*, 4562–4573; c) M. Pavelka, M. F. A. Lucas, N. Russo, *Chem. Eur. J.* **2007**, *13*, 10108–10116; d) M. F. A. Lucas, M. Pavelka, M. E. Alberto, N. Russo, *J. Phys. Chem. B* **2009**, *113*, 831–838; e) A. Melchior, M. Tolazzi, J. M. Martínez, R. R. Pappalardo, E. Sánchez Marcos, *J. Chem. Theory Comput.* **2015**, *11*, 1735–44.

[22] *F. R. Hertley*, in *The Chemistry of Palladium and Platinum*, *ed*. P. L. *Robinson*, *Applied Science*, *London*, ***1973***, vol. *14*, p.*458*.

[23] A. J. M. Duisenberg, L. M. J. Kroon-Batenburg, A. M. M. Schreurs, *J. Appl. Crystallogr*., **2003**, *36***,** 220-229.

[24] G.M. Sheldrick, SADABS, Absorption Correction Program, University of Göttingen, Germany, **2008**

[25] M.C. Burla, R. Caliandro, B. Carrozzini, G. L. Cascarano, C. Cuocci, C. Giacovazzo, M. Mallamo, A. Mazzone & G. Polidori, *J. Appl. Crystallogr*., **2015**, *48*, 306-309.

[26] G.M. Sheldrick, *Acta. Crystallogr*. **2015**, *C71*, 3-8.

[27] A. L. J. Spek, *J. Appl. Crystallogr*. **2003**, *36*, 7–13.

[28] C. F. Macrae, I. J. Bruno, J. A. Chisholm, P. R. Edgington, P. McCabe, E. Pidcock, L. Rodriguez-Monge, R. Taylor, J. van de Streek & P. A. Wood, *J. Appl. Cryst*., **2008**, *41*, 466-470.

[29] M. C. Burla, R. Caliandro, M. Camalli, B. Carrozzini, G. L. Cascarano, C. Giacovazzo, M. Mallamo, A. Mazzone, G. Polidori & R. Spagna, *J. Appl. Crystallogr*. **2012**, *45* , 357-361.

[30] D. Andrae, U. Häußermann, M. Dolg, H. Stoll, H. Preuß, *Theor. Chim. Acta* **1990**, *77*, 123–141.

[31] M. J. Frisch, G. W. Trucks, H. B. Schlegel, G. E. Scuseria, M. A. Robb, J. R. Cheeseman, G. Scalmani, V. Barone, B. Mennucci, G. A. Petersson, et al., *Gaussian, Inc., Wallingford CT*, **2009**.

[32] a) A. Melchior, E. Sánchez Marcos, R. R. Pappalardo, J. M. Martínez, *Theor. Chem. Acc*. **2011**, *128*, 627–638; b) F. Endrizzi, A. Melchior, M. Tolazzi, LF Rao *Dalton Trans.* **2015**, *44*, 13835-13844; c) P. Di Bernardo, P.L. Zanonato, F. Benetollo, A. Melchior, M. Tolazzi, L. Rao *Inorg. Chem*. **2012**, *51*, 9045–55; d) A. Melchior, E. Peralta, M. Valiente, C. Tavagnacco, F. Endrizzi, M. Tolazzi *Dalton Trans*. **2013**, *42*, 6074–6082; e) S. Del Piero, R. Fedele, A. Melchior, R. Portanova, M. Tolazzi, E. Zangrando, A. Melchior, *Inorg. Chem*. **2007**, *46*, 1406–1406; f) C. Comuzzi, A. Melchior, P. Polese, R. Portanova, M. Tolazzi *Inorg. Chem*. **2003**, *42*, 8214–8222.

[33] J. Tomasi, B. Mennucci, R. Cammi, *Chem. Rev.* **2005**, *105*, 2999–3093.

[34] N. Margiotta, N. Denora, S. Piccinonna, V. Laquintana, F. M. Lasorsa, M. Franco, G. Natile, *Dalton Trans*.**, 2014**, *43*, 16252-16264.

[35] R. T. Boeré, C. J. Willis, *Inorg. Chem*. **1985**, *24*, 1059-1065.

[36] a) R.F.V. de Souza, E. M. Sussuchi, W. F. De Giovani, *vol 33, issue 7,* **2003** "Synthesis and reactivity in inorganic and metal-organic chemistry" 1125-1144; b) K. Lemanska, H. Szymudiak, B. Tyrakowska, R. Zielinski, A. E. M. F. Soffers, I. M. C. M. Rietjens, *Biol. Med*, **2001**, *31*, 869−881.

[37] G. K. Anderson, M. J. Arendse, N. P. Rath, *Inorg. Chem*. **1999**, *38*, 5864–5869.

[38] a) J. Zhou, L. Wang, J. Wang, N. Tang, *Transition Met. Chem. (Dordrecht, Neth.),* **2001**, *26*, 57−63; b) D. Malesev, V. Kunti, *J. Serb. Chem. Soc.*, **2007,** 72, 921-939.

[39] K. Nakamoto, Infrared and Raman Spectra of Inorganic and Coordination Compounds, Wiley, New York **1997**, 5th edit., Pt B, pp. 7, 169 and 172.

[40] L. J. Farrugia, *J. Appl. Crystallogr*. **2012**, *45*, 849-854.

[41] P. Bergamini, E. Marchesi, V. Bertolasi, M. Fogagnolo, L. Scarpantonio, S. Manfredini, S. Vertuani, A. Canella, *Eur. J. Inorg. Chem*., **2008**, 529–537.

[42] D. C. Burns, D. A. Ellis, R. E. March, *Magn. Reson. Chem*., **2007**, *45*, 835-845.

[43] P. Donato, D. Raneri, G. Guglielmo, P. Ficarra and R. Ficarra, *J. Pharm. Biomed. Anal*., **2004**, *35*, 389–397.

[44] a) T. Matsuura, T. Takemoto and R. Nakashima, *Tetrahedron*, **1973**, *29*, 3337–3340; b) I. Yokoe, K. Higugi, Y. Shirataki and M. Komatsu, *Chem. Pharm.Bull*., **1981**, *29*, 894–898; c) M. Sisa, S. L. Bonnet, D. Ferreira, J. H. Van der Westhuizen, *Molecules* **2010**, *15*, 5196-5245.

[45] C. Rice-Evans, Flavonoids antioxidants, *Curr. Med. Chem*., **2001**, *8*, 797–807.

[46] a) P. Chou, D. McMorrow, T. J. Aartsma and M. Kasha, *J. Phys. Chem*., **1984**, *88*, 4596–4599; b) E. Biagtan, E. Goldberg, R. Stephens, E. Valeroso and J. Harmon, *Nucl. Instrum. Methods Phys. Res., Sect. B*, **1996**, *114*, 88–90; c) S. Carturan, A. Quaranta, G. Maggioni, M. Bonafini and G. Della Mea, *Sens. Actuators, A*, **2004**, *113*, 288–292; d) V. V. Shynkar, A. S. Klymchenko, C. Kunzelmann, G. Duportail, C. D. Muller, A. P. Demchenko, J.-M. Freyssinet and Y. Mely, *J. Am. Chem. Soc*., **2007**, *129*, 2187–2193 and references therein; e) B. Gerard,G. Jones II and J.A. Porco, Jr., *J. Am. Chem. Soc*., **2004**, *126*, 13620–13621; f) B. J. Schwartz, L. A. Peteanu and C. B. Harris, *J. Phys. Chem.*, **1992**, *96*, 3591–3598 and references therein.

[47] S. Protti, A. Mezzetti, C. Lapouge, J.-P. Cornard, *Photochem. Photobiol. Sci*., **2008**, *7*, 109–119.

[48] S. L. Saraf, T. J. Fish, A. D. Benninghoff, A. A. Buelt, R. C. Smith, L. M. Berreau, *Organometallics*, **2014**, *33*, 6341−6351.

[49] a) K. Grubel, S. L. Saraf, S. N. Anderson, B. J. Laughlin, R. C. Smith, A. M. Arif, L. M. Berreau, *Inorg. Chim. Acta*, **2013,** *407*, 91–97; b) K. Grubel, A. R. Marts, S. M. Greer, D. L. Tierney, C. J. Allpress, S. N. Anderson, B. J. Laughlin, R. C. Smith, A. M. Arif, L. M. Berreau, *Eur. J. Inorg. Chem*., **2012**, 4750–4757.

[50] J. S. Pap, J. Kaizer, G. Speier, *Coord. Chem. Rev*. **2010**, *254*, 781–793.

[51] M. S. Davies, S. J. Berners-Price, T. W. Hambley, *Inorg. Chem.* **2000**, *39*, 5603–5613.

[52] a) J. K. C. Lau, D. V. Deubel, *J. Chem. Theory Comput.* **2006**, *2*, 103–106; b) D. V Deubel, *J. Am. Chem. Soc.* **2004**, *126*, 5999–6004.

[53] a) J. Vinje, E. Sletten, J. Kozelka, *Chem. - A Eur. J.* **2005**, *11*, 3863–3871; b) G. Lamm, G. R. Pack, *Proc. Natl. Acad. Sci. U.S.A* **1990**, *87*, 9033–9036.

[54] S. J. Berners-Price, T. G. Appleton, in (Eds.: L.R. Kelland, N.P. Farrell), Humana Press, Totowa, NJ, **2000**, pp. 3–35.

[55] M. E. Alberto, V. Butera, N. Russo *Inorg. Chem*. **2011**, *50*, 6965–6971.

[56] a) A. A. Recio Despaigne,, J. G. Da Silva, P. R. da Costa, R. G. dos Santos, H. Beraldo, *Molecules* **2014**, *19*, 17202-17220; b) J. J. Wilson, S. J. Lippard, *J. Med. Chem*. **2012**, *55*, 5326−5336.

Supplementary Information for Publication Online

Click here to download Supplementary Information for Publication Online: Pt-polyph_ESI.docx

CIF File(s) (REQUIRED if paper describes X-ray crystal structures)

Click here to download CIF File(s) (REQUIRED if paper describes X-ray crystal structures): pt_7_sq (1430059).cif

CIF File(s) (REQUIRED if paper describes X-ray crystal structures)

Click here to download CIF File(s) (REQUIRED if paper describes X-ray crystal structures): pt_9 (1430058).cif

CIF Validation Report(s) (RECOMMENDED if paper describes X-ray crystal structures)

Click here to download CIF Validation Report(s) (RECOMMENDED if paper describes X-ray crystal structures): checkcif Pt 7 sq.p

CIF Validation Report(s) (RECOMMENDED if paper describes X-ray crystal structures)

Click here to download CIF Validation Report(s) (RECOMMENDED if paper describes X-ray crystal structures): checkcif Pt 9.pdf